Ablation of VEGFA following a lumbar intervertebral disc injury attenuates intradiscal neurovascular features and prevents chronic low back pain symptoms

Authors: *Ryan S. Potter[1],*Hong J. Moon[3], *Sade W. Clayton[2], Remy E. Walk[2], Addison L. Liefer[2], Liufang Jing[2], Amber N. Stratman[3], Lori A. Setton[1,2,4], Munish C. Gupta[3], Simon Y. Tang[1,2,4]

***These authors led the study equally.**

Affiliations:

[1] Department of Mechanical Engineering and Materials Science, Washington University in St. Louis
[2] Department of Biomedical Engineering, Washington University in St. Louis
[3] Department of Cell Biology and Physiology, Washington University School of Medicine
[4] Department of Orthopaedic Surgery, Washington University School of Medicine

Corresponding author: Simon Tang (simon.tang@wustl.edu)

One Sentence Summary:
VEGFA critically mediates the infiltration of neurovascular features into the degenerating intervertebral disc, and the ablation of VEGFA prevents chronic low back pain behavior.

Keywords:
VEGFA, intervertebral disc injury, low back pain, neurovascular features, preclinical model

Abstract

There are currently no therapies for the staggering disability and public health costs of chronic low back pain (LBP). Innervation of the degenerating intervertebral disc (IVD) is suspected to cause discogenic LBP, but the mechanisms that orchestrate the IVD's neo-innervation and subsequent symptoms of LBP remain unknown. We hypothesize that Vascular Growth Endothelial Factor-A (VEGFA) critically mediates the neurite invasion in the IVD and contributes to prolonged LBP. Initiating IVD degeneration through a mechanical injury, we evaluated the progression of neurovascular features into the IVD, as well as resultant LBP symptoms and locomotive performance at acute (3-weeks) and prolonged (12-weeks) time points following IVD injury. To determine the role of VEGFA, we used a mouse model with ubiquitous inducible recombination of the floxed VEGFA allele (UBC-Cre^{ERT2}; VEGFA$^{fl/fl}$). The ablation of VEGFA attenuated the neurite and vessel infiltration into the degenerating IVD, and the VEGFA-null animals exhibited alleviated mechanical allodynia and improved locomotive performance. To determine the effects of IVD-derived VEGFA on endothelial cells and neurons, we cultured HMEC-1 endothelial cells and SH-SY5Y neurons using conditioned media from VEGFA-silenced (siRNA) human primary IVD cells stimulated by IL1β. The endothelial cells and neurons exposed to the secretome of the VEGFA-silenced IVD cells exhibited reduced growth, suggesting that the inhibition of IVD-derived VEGFA may be sufficient to attenuate intradiscal neurovascular features. Together, we show that VEGFA orchestrates the growth of intradiscal vessels and neurites that cause low back pain and impaired function, and the inhibition of VEGFA can prevent prolonged low back pain.

52 **INTRODUCTION**

53 Low back pain (LBP) is a prevalent, debilitating, costly, and multifactorial condition worldwide,
54 imposing substantial global and economic burdens [1-3]. LBP affects 30–80% of the population and
55 increases with age [4]. It is the leading cause of years lived with disability and contributes an estimated
56 $50 to $100 billion USD annually in direct healthcare costs [5,6] Chronic LBP is commonly associated
57 with intervertebral disc (IVD) degeneration, which occurs due to aging, genetic predisposition, and
58 mechanical stress [7-10]. Degeneration leads to structural and biochemical changes—such as loss of
59 hydration, inflammation, and matrix breakdown—that impair disc function [11-14]. However, due to the
60 complexity of these changes, it remains unclear which specific features of degeneration are responsible
61 for pain [15].

62

63 Innervation has been identified in painful human intervertebral discs, suggesting a role for aberrant nerve
64 growth in discogenic pain [16]. VEGFA (Vascular Endothelial Growth Factor A) has canonical roles in
65 neurovascular growth and its enhanced expression during injury may thus facilitate this pathological
66 growth [17]. VEGFA is a potent signaling protein known for its role in promoting angiogenesis and
67 neurogenesis. It stimulates endothelial and neural cells, influencing processes such as cell proliferation,
68 migration, and survival [18,19]. While VEGFA has known roles in both vascular and neural support, its
69 function in IVD injury models and its potential to initiate or sustain discogenic pain remain unresolved.
70 We hypothesized that the ablation of VEGFA attenuates neurite growth and vascularization into the
71 injured IVD, mediates structural and functional deficits of the IVD, and alleviates ensuing low back pain
72 symptoms.

73

74 To investigate the role of VEGFA in IVD degeneration and pain, we utilized a mouse model with an

inducible ablation of VEGFA and we created an injury in the lumbar IVD to model degeneration. We subsequently quantified pain-related symptoms such as mechanical sensitivity and locomotor deficits [20]. Because VEGFA is also a critical regulator of vascular growth, we assessed neo-vascularization into the injured IVD along with neural infiltration to better understand the relationship between vascular and neural response in disc degeneration. In human cells, we performed co-culture experiments determine the role of IVD-produced VEGFA on neuron and endothelial cell growth.

Our findings demonstrate that VEGFA plays a central role in promoting neurovascular ingrowth into the degenerating intervertebral disc, contributing to chronic low back pain. The ablation of VEGFA significantly reduced neurite and blood vessel infiltration into the injured disc and alleviated mechanical allodynia and locomotor deficits in mice. In vitro, endothelial cells and neurons exposed to conditioned media from VEGFA-silenced IVD cells exhibited diminished growth, reinforcing VEGFA's role as a key mediator of discogenic pain pathways. These results demonstrate that targeted inhibition of VEGFA can suppress intradiscal vessels and neurites that cause low back pain and impaired function, and this results in the prevention of chronic low back pain.

RESULTS

Removal of VEGFA Blunts Intradiscal Invasion of Neurovascular Structures

In WT animals, the injured IVD was infiltrated by PGP9.5+ neurons and by endomucin+ vessels VEGFA ablation significantly blunted these neuronal and vascular features. Immunofluorescence images from 50µm thick sections (Figure 1A-B) showed reduced neural and vascular structures in VEGFA-null mice compared to WT particularly in the region around the outer AF. Quantitative measurements of structural length and depth (Figure 1C-F) revealed significant differences in neurite length (p=0.01), vessel length (p=0.004), neurite depth (p=0.002), and for vessel depth (p=0.047) due to VEGFA removal. Post hoc analysis reveals differences between the WT and VEGFA-null IVDs in neurite depth at 3 weeks (p=0.001) and in vessel length at 12 weeks (p=0.01). These findings show that VEGFA is crucial for instigating the neural and vascular structures in IVDs following injury. VEGFA ablation can limit the penetration into- and the propagation within- of these structures of the disc.

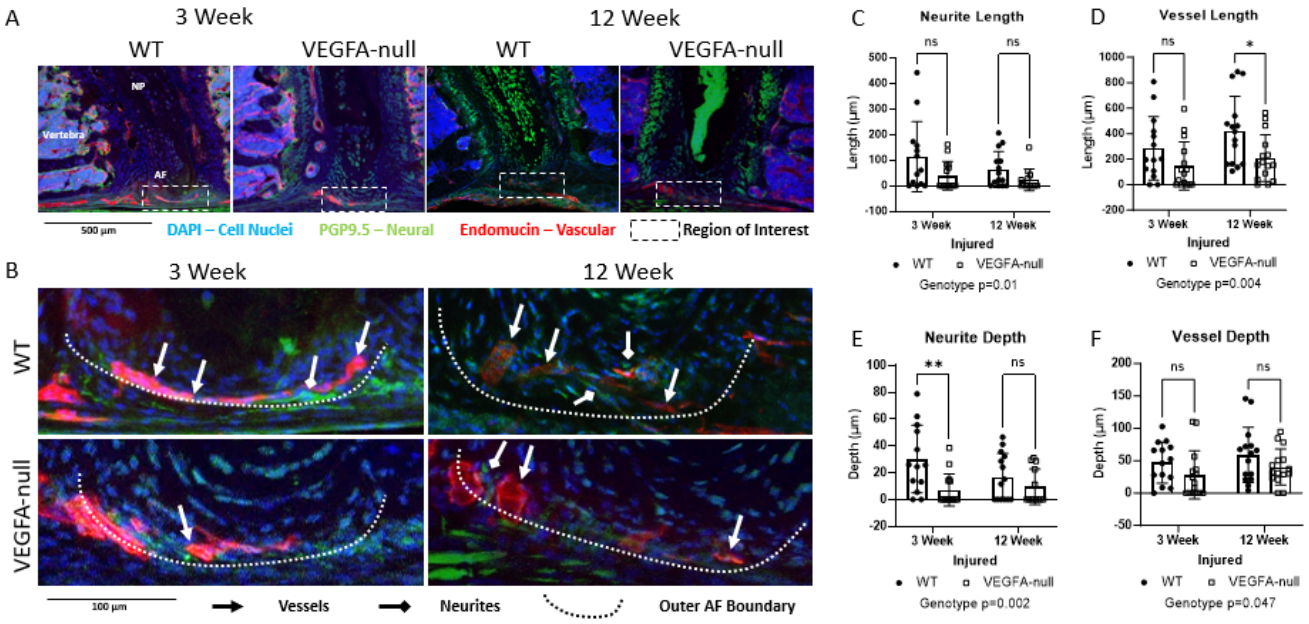

Fig. 1: Removal of VEGFA Blunts Intradiscal Invasion of Neurovascular Structures Following IVD Injury. A) IHC of dorsal sides of the injured lumbar IVD with the nuclei (DAPI) in blue, neuronal

features (PGP9.5) in green and vascular features (Endomucin) in red. The ROI is boxed with dotted lines. B) Outer AF ROI with key features notated C-F) VEGFA loss reduces neurite lengths (p=0.01) and vessel lengths (p=0.004) across both post-injury time points. Likewise, the neurite penetration depth (p=0.002) and vessel penetration depth (p=0.047) are blunted by VEGFA removal. Data are presented as mean ± standard deviation.

VEGFA Is Essential for the Spatial Colocalization of Intradiscal Nerves and Vessels

The spatial proximity of intradiscal nerves and vessels are disrupted by VEGFA ablation. Immunofluorescence images reveal the distribution of neural (PGP9.5, green) and vascular (Endomucin, red) structures highlighting the regions of interest around the outer annulus fibrosus (AF) and overlapping lengths relative to neurites, due to their rarer presence in the disc Figure 2A-B. The colocalization analysis show that the WT injured IVDs have neurites with a large amount of vessels in its proximity. The removal of VEGFA in the IVDs 3 weeks following injury prevented neurites from infiltrating the IVD (Figure 2-2C), but this difference between KO and WT animals did not persist at 12 weeks after injury. However, the loss of VEGFA did not deter Endomucin+ vessels from penetrating the injured IVD at both time points (Figure 2D). The spatial overlap analysis between neurites and vessels (Figure 2E) show that VEGFA ablation dramatically reduces the amount of neurites near vessels (p=0.007). After adjusting for the length of the neurites, this observation remains robust independent of the basal level of neurites in each animal (p=0.008; Figure 3F).

The lack of difference between the depth and length ratios between neurites and vessels indicates that once initiated, VEGFA does not appear to affect the propagation of these features (Figure 2G; 2H). These findings highlight the critical role of VEGFA in the initiation of neural and vascular features in the IVD.

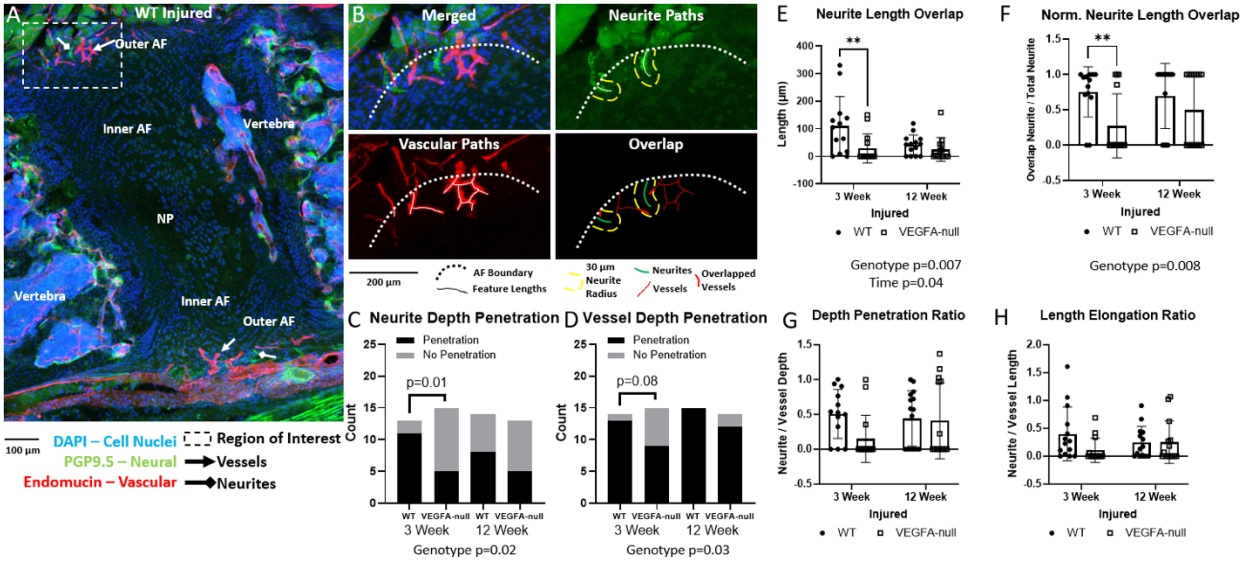

Fig. 2: VEGFA is Essential for the Colocalization of Intradiscal Nerves and Vessels Initiation. A) WT injured disc showing key features of the IVD and a ROI for analysis B) Graphic representation of how spatial colocalization analyses quantified the amount of neurites that were in proximity of vessels with a 30 µm region. C-D) Loss of VEGFA significantly reduced the number injured IVDs that experienced infiltrating neurites 3 weeks after injury (p=0.01) in VEGFA-null at 3 weeks. Neurite penetration (p=0.02) and vessel penetration (p=0.03) both show a significant decrease in VEGFA-null groups. E) VEGFA ablation reduced the amount of vessel-adjacent neurites (p=0.007), and was dependent on amount of time following injury (p=0.04). F) The effect of VEGFA loss on preventing neurite-vessel spatial coupling persevered even when accounting for varying intradiscal neurite lengths between different animals (p=0.008), confirming that this is a local phenomenon conserved across animals. G-H) The lack of difference in the depth penetration and length elongation ratios suggest that, on average, once the neurites have initiated, the loss of VEGFA did not appear to affect their propagation. Statistical model C-D: Fisher's exact test. Statistical model E-H: 2 factor ANOVA with Fisher LSD post-hoc comparisons. E-H Data are presented as mean ± standard deviation.

Depletion of VEGFA Suppresses the Expression of Pain-related Ion Channels in the DRG

Quantitative measurements of CTCF of mice DRGs (Figure 3B-D) revealed a significant reduction in TRPA1 fluorescence (p=0.04) due to VEGFA removal following injury. No significant changes were measured in TRPV1 CTCF levels from VEGFA ablation indicating that TRPV1 is unaffected by VEGFA levels.

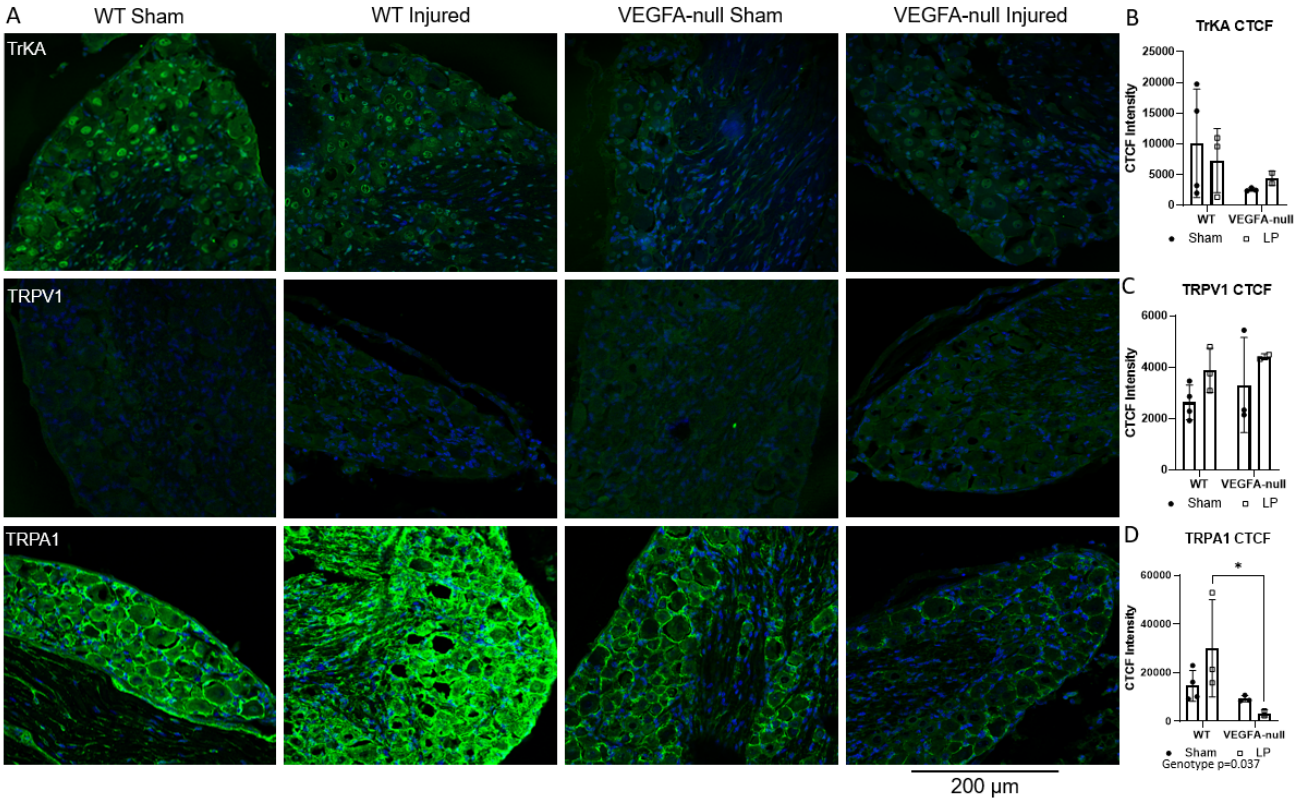

Fig. 3: VEGFA Inhibition Reduces the Expression of Ion Channels Associated with DRG pain. A) TrKA (top), TRPV1 (middle), and TRPA1 (bottom) in green and DAPI in blue were quantified. B-D) Corrected total cell fluorescence (CTCF) for each pain related ion channel shows VEGFA ablation regulated TRPA1 expression (p=0.037).

157 **Ablation of VEGFA Alleviates Mechanical sensitivity and Locomotive Function**

158 *Loss of VEGFA Attenuates Mechanical, but Not Hot or Cold, Sensitivity*

159 The WT animals exhibited mechanical sensitivity measured by the Von Frey filament test at both 3 and
160 12 weeks after intervertebral disc injury. Ablation of VEGFA alleviated this impairment at the 12-week
161 time point (p=0.001, Figure 4A). The electronic Von Frey filament test also revealed that there is a
162 greater mechanical sensitivity on the side of the surgical approach. VEGFA removal specifically
163 alleviated the mechanical sensitivity of the injured side, without modifying the contralateral side. No
164 notable changes observed in heat or cold sensitivity.

165 *VEGFA Ablation Improves Rotarod Performance, but Does Not Affect Passive Function*

166 We also evaluated locomotive performance through an active challenge of locomotive function,
167 measured through the rotarod assay, longitudinally, every three weeks up to 12 weeks after injury. The
168 longitudinal Rotarod test (Figure 4D) reveals that VEGFA-null mice exhibit significantly maintained
169 latency to fall at 9 and 12 weeks compared to impaired WT (p=0.004), highlighting impaired motor
170 coordination over time (p=0.003). In the Open Field test, total distance traveled (Figure 4E) and rearing
171 counts (Figure 4F) are not significantly different between genotypes, suggesting comparable levels of
172 exploratory behavior and general activity.

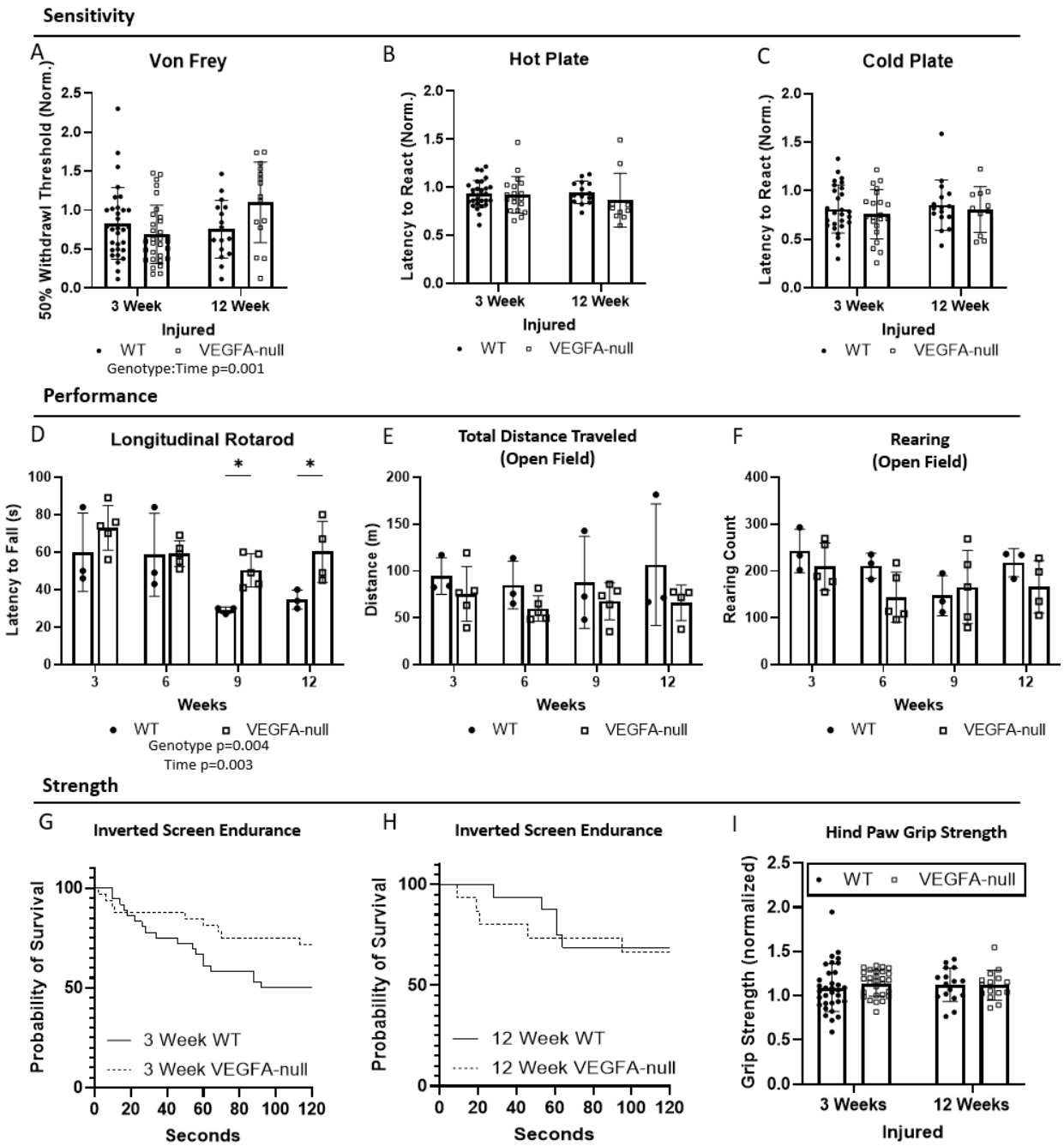

Fig. 4: VEGFA Ablation Improves Mechanical Sensitivity and Performance A) Mechanical sensitivity shows a statistically significant interaction between genotype and time (p=0.001) with a worsening effect seen in WT leading to a chronic sensitivity and an improving effect in VEGFA-null over time that recovers near baseline. B-C) Temperature sensitivity changes were not statistically

178 significant. D) Longitudinal measures of performance included rotarod which shows genotype
179 (p=0.004) and time (p=0.003) statistical significance, indicative of a VEGFA rescue of a more chronic
180 progression of performance impairment. E-F) Open field measures of total distance and rearing are not
181 statistically significantly different. G-H) Inverted screen endurance at 3 and 12 weeks was not
182 statistically significantly different. I) Hind paw grip strength remained unchanged. Statistical model A-
183 F, I: Linear mixed effects with genotype and time as factors with post-hoc LSM with Sidak correction.
184 G-H Mantel-Cox test. A-F, I Data are presented as mean ± standard deviation.

Assay	Sex M/F	Tamoxifen +/-	Naïve/Sham
Von Frey	0.94	0.63	0.66
Grip Strength	0.09	0.92	0.07
Inverted Screen	0.65	0.33	0.64
Cold Sensitivity	0.52	0.06	0.40
Heat Sensitivity	0.44	0.47	0.57
Rotarod	0.34	0.43	0.25
Distance (Open Field)	0.33	0.27	0.18
Rearing (Open Field)	0.25	0.32	0.59
Neurite Length	0.08	NA	NA
Vessel Length	0.19	NA	NA
Neurite Depth	0.51	NA	NA
Vessel Depth	0.15	NA	NA

185 **Table S4: Behavioral and Neurovascular Significance Values for Sex, Tamoxifen, and Naïve/Sham** P-values showing
186 the lack of significant differences (p>0.05) between Male and Female, Tamoxifen +/-, and Naïve and Sham surgery for the
187 behavioral, neuronal, and vascular assays. P-values from the Linear Mixed Effects statistical model. Factors without
188 samples for comparison are shown as NA.
189

190 *VEGFA Removal Does Not Affect Measures of Strength*

191 Strength assessments include inverted screen endurance and hind paw grip strength. The inverted screen
192 endurance test, indicated by the survival analysis, showed that VEGFA-null mice have similar
193 probabilities of hanging on compared to WT at both 3 weeks (Figure 4G) and 12 weeks (Figure 4H).
194 Hind paw grip strength (Figure 4I) shows no differences, indicative of no compromise in muscle
195 function from VEGFA ablation.

196 Overall, these findings show that VEGFA-null mice have improved recovery of mechanical
197 sensitivity and avert the transition to chronic sensitivity seen in the WT while also avoiding the
198 performance deficits in WT at chronic time points.

199

200 **Ablation of VEGFA Does Not Affect structure, function, or degeneration of the IVD**

201 *Loss of VEGFA Does Not Affect the Histopathic Degeneration of the IVD*

202 CEμCT analysis of the IVDs 3 weeks after injury reveals significant deterioration of the IVD structure.
203 By using a contrast enhancing agent, Ioversol, the injury can be observed on the ventral side of the outer
204 AF as a progressively higher attenuating regions that mark the fibrous scar tissues (Figure 5A). The
205 injured IVDs also exhibit a loss of NP attenuation, measured by NI/DI, demonstrating the loss of the
206 water retaining ability of the NP ($p=0.03$, Figure 5B). The ablation of VEGFA does not affect these
207 injury-mediated changes in degeneration. A narrowing of the intradiscal space measured by Disc height
208 index (DHI), a hallmark of IVD degeneration, is apparent in the injured discs ($p=0.01$, Figure 5C).
209 Surprisingly, there was not a change in NP volume either due to injury or VEGFA ablation. Structurally,
210 injury increases degenerate features including decreased NP hydration and a narrowing DHI while
211 VEGFA ablation shows promising trends to recover these injury induced changes. Noticeably, there was

212 a spectrum of structural adaptations that may be due to variations in the surgical injury due to needle
213 depths, approach angles differences, and surgical conditions.

214 *Injury to the IVD Does Not Impair Its Mechanical Function*

215 Dynamic compression of IVDs 3 weeks post injury show no distinct responses to injury or impact from
216 VEGFA ablation. The stiffness measurements show no significant differences between WT and
217 VEGFA-null groups, both in sham and injured conditions (Figure 5D). Likewise, the dissipation factor
218 indicates a similar response with no appreciable changes from injury or VEGFA loss (Figure 5E). These
219 findings show that the degeneration that occurs at 3 weeks after injury does not yet impair its mechanical
220 function.

221 *VEGFA Loss Does Not Rescue the Degenerative Changes Caused by Injury*

222 Histopathological scoring (Figure 5H) revealed the destructive effect of a needle stab on the
223 compartments in the disc, including decreased NP cell density and changes in cellular morphology,
224 disruption of the AF concentric lamellar structures with increased cellularity and presence of clefts,
225 along with thinning and disruptions in the endplate cartilage, and structural disorganization in the
226 boundary regions. Scores for injured groups averaged near 26 out of 36 maximum while sham controls
227 were near 11 with the greater degeneration in the injured discs ($p < 0.0001$) compared to the sham
228 animals with no IVD injury. Statistical differences from VEGFA removal were not present. Mechanical
229 injury dramatically changed all compartments of the disc with the largest effects on the AF followed by
230 NP as expected based on the AF stab model while sham scores indicate a moderate degeneration from
231 the exposure of the disc and likely disruption of surrounding soft tissues.

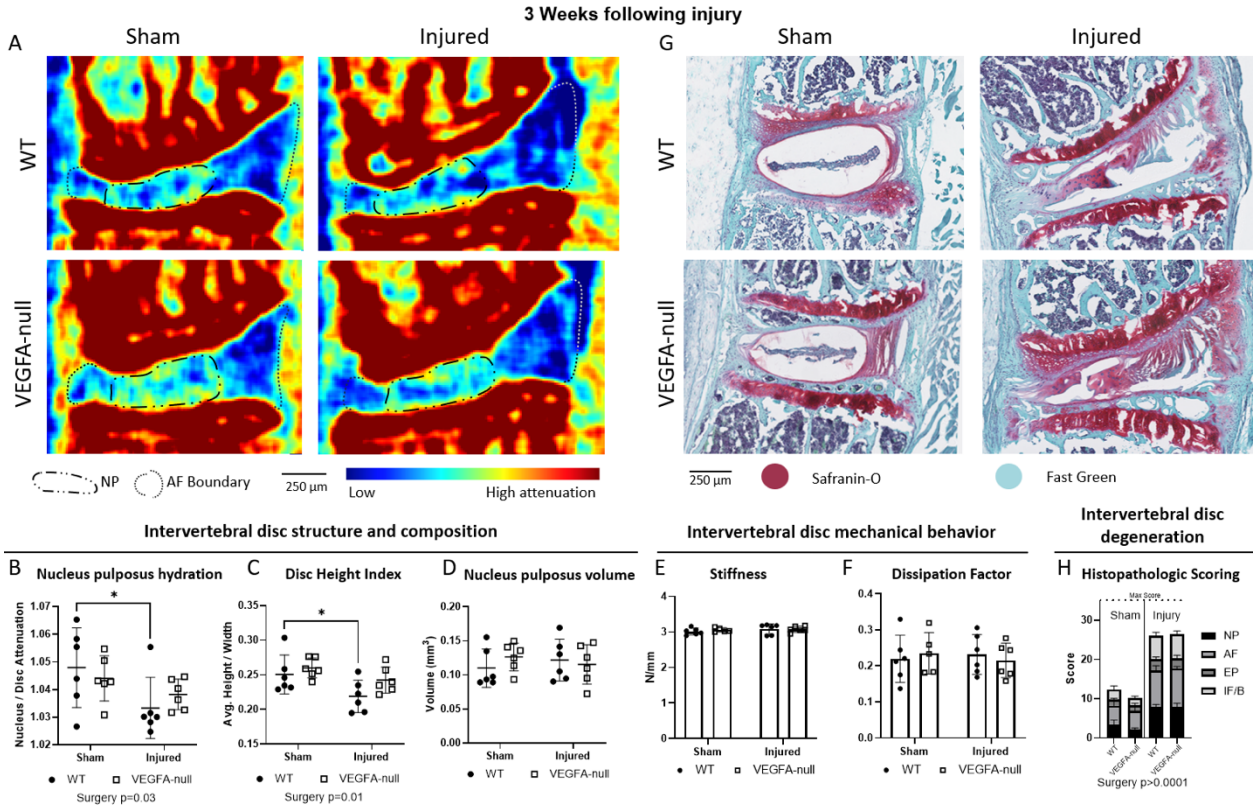

Fig. 5: Loss of VEGFA Does Not Alter Structural, Mechanical, or Histopathologic Degeneration to the Injured IVD. A) IVD structure and compositional changes via CEµCT show that B) injury decreased NP hydration (p=0.03), indicated by the decreased attenuation of the NP, C) injury decreased disc height index, DHI, (p=0.01) compared to sham, and D) no effect of NP volume was observed. VEGFA removal showed a trend towards Sham levels on the DHI indicating a potential protection against hydration loss. Changes to mechanical behavior were not observed in E) stiffness and F) dissipation factor, indicating that tissue level mechanics were not changed by injury or VEGFA removal at this 3-week post injury time point. G) Histological images stained with Safranin-O and Fast Green show IVD degeneration H) with histopathologic scoring showing a highly statistically significant effect of injury (p<0.0001) with no appreciable differences due to VEGFA loss in nucleus pulposus, annulus fibrosis, end plate, or the interface/boundary demonstrating the pathophysiological response from needle puncture. Data are presented as mean ± standard deviation.

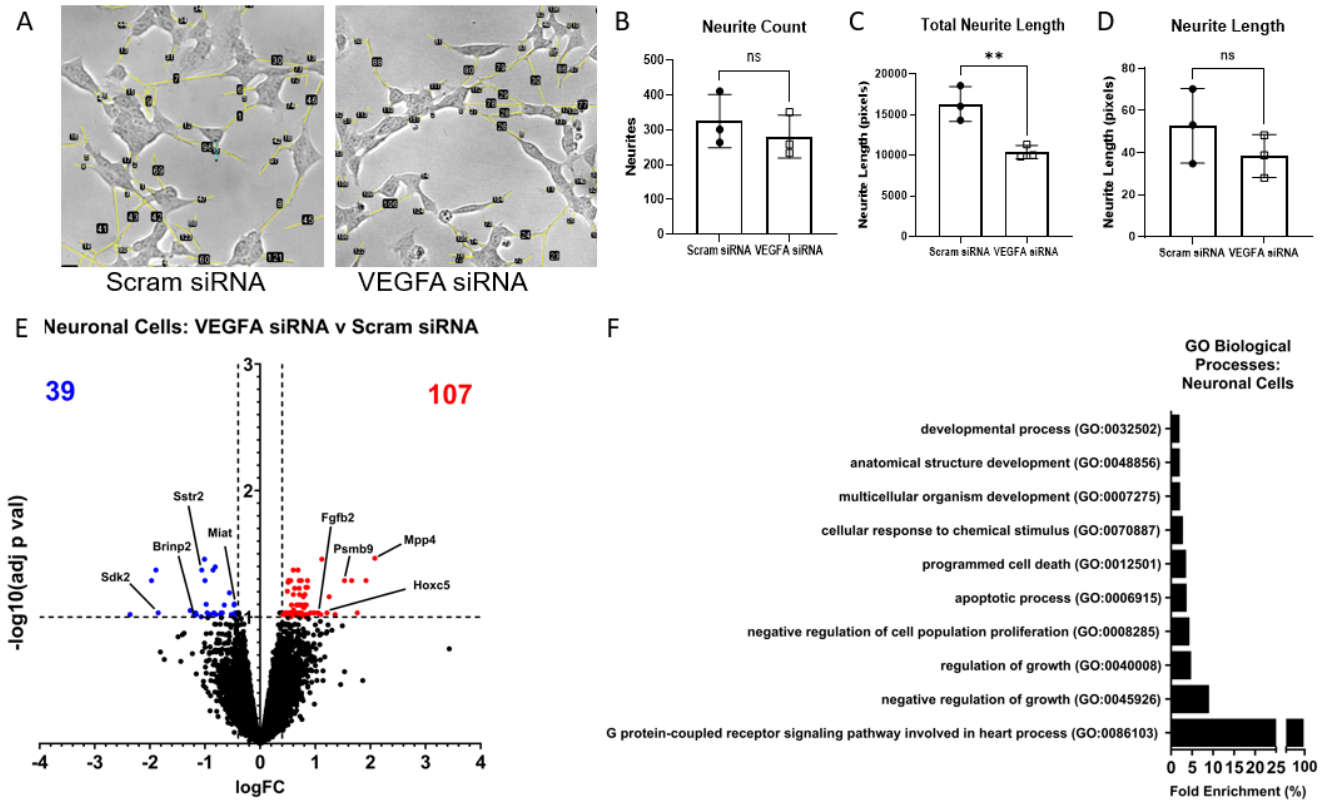

Fig. 6: VEGFA Inhibition Reduces *in vitro* Neurite Activity and Alters Gene Transcription A) Neurite extension assay after treating neuronal cells with media collected from IL-1B stimulated and siRNA transfected human disc cells shows inhibition of neurites from VEGFA siRNA. B-D) Quantification of neurite morphology showing functional suppression with VEGFA siRNA E) RNA-seq showing 146 differentially expressed genes and F) key biological processes regulated by VEGFA siRNA. NCs co-cultured with IL1β- NAIVE DISC CELLS, (IL1β- NAIVE DISC CELLS)NC showed undifferentiated cell possessing few short projections and cluster together (Figure 5A, open arrows), while NCs co-cultured with IL1β+SCRAM siRNA, (IL1β+SCRAM siRNA)NC and NCs co-cultured with IL1β+VEGFA siRNA, (IL1β+VEGFA siRNA)NC showed differentiated cells having many extensive projections (Figure 5A, closed arrows). Total neurite number from 1. (IL1 β-NAIVE DISC

258 CELLS)NC, 2. (IL1β+SCRAM siRNA)NC and 3. (IL1β+VEGFA siRNA)NC was 194.7 ± 52.6, 325.3
259 ± 76.5 and 281.0 ± 61.8 respectively. 1 vs 2 and 2 vs 3 showed significant difference (p=0.01 and
260 p=0.04). Total neurite length was 4094.2 ±1185.0, 16283.5 ± 2149.6 and 10376.5 ± 813.4 respectively.
261 1 vs 2 and 2 vs 3 showed significant difference (p=0.02 and p=0.02).

262 **Silencing VEGFA RNA in Human IVD Cells Attenuates the Growth of Co-Cultured Neuronal**
263 **and Endothelial Cells**

264 Transfecting human IVD cells with Vegfa-specific small interfering RNA (siRNA) suppressed their
265 subsequent production of the VEGFA protein expression by 57.4% when stimulated with IL-1β (Figure
266 S8). Coculturing these Vefga-siRNA transfected, IL-1β stimulated IVD cells with SH-SY5Y neurons
267 maintained the neuron morphology but blunted the growth of the axonal extensions (Figure 6A).
268 Although the number of neurites and their averaged lengths did not change for co-cultured neurons
269 (Figure 6B), the total neurite length increased in the group cultured with Vegfa-intact IVD cells (Figure
270 6C, D). There was no change in average neurite length (Figure 6D). RNA sequencing revealed that
271 neurons cultured with Vegfa-deficient IVD cells expressed 39 downregulated and 107 upregulated
272 DEGs (Figure 6E). Gene ontology analysis determined the most enriched biological process from the
273 DEGs involved the regulation of general cell processes, e.g. GCPR signaling pathway involved on hear
274 process (*Ednra, Chga, Ramp3*), Negative regulation of growth (*DCC, GREM1, STC2, MYOZ1, MT1F,*
275 *BST2, MT1X, BCL2*), and the Negative regulation of cell population proliferation (*GREM1, PTPN14,*
276 *DHRS2, SSTR2, SCG2, SERPINF1, IGFBP3, OVOL1, ADM, IGFBP7, BCL2, S100A11*). Notably, a
277 number of DEGs were specific to cell growth inhibition (*SSTR2, S100A11), immune* cells and
278 inflammation (*CXCR4, FGFB2, IL32)*, and neuronal cell functions (*DCC, SDK2*, *ASTN2*).
279

280 We also co-cultured siRNA transfected IVD cells with HMEC-1 cells. Endothelial cells (EC) cocultured
281 with Vegfa-silenced human IVD cells were less capable of forming closed tubes, a measure angiogenesis
282 (Figure 7A). ECs cultured with Scram siRNA significantly developed a higher number of closed loops
283 than ECs cultured with Vegfa siRNA (16.3 ± 4.4 vs 7.3 ± 3.1, p=0.04) after 6 hours culturing. (Figure
284 7B). RNAseq uncovered 175 downregulated and 0 upregulated DEGs due to Vegfa siRNA transfection
285 when compared to human IVD cells transfected with Scram siRNA (Figure 7C). Gene ontology analysis
286 determined the most enriched biological process from the DEGs involved in vessel and vasculature
287 related process, e.g. Lymph vessel development (*NR2F2, TBX1, SOX18, EFNB2,HEG1*), Blood vessel
288 morphogenesis (*TNFAIP2, EFNB2, HEG1, PRKACA, NRARP, TBX1, SOX4, NR2F2, AKT1, QKI,*
289 *SMAD7, SOX18, VEGFB*), and Regulation of neuron projection development (*EFNB2, CDK5R1, RYK,*
290 *RAPGEF1, CARM1, AKT1, PLZNA1, NCS1, DVL1, SLK, STK24, BRSK2, ADNP*). Interestingly,
291 Canoincal Wnt signaling pathway was also an enriched biologically pathway and Wnt signaling plays
292 an important role in endothelial cell proliferation, survival, differentiation and response to mechanical
293 forces due to shear stress from blood flow.[20,21]
294

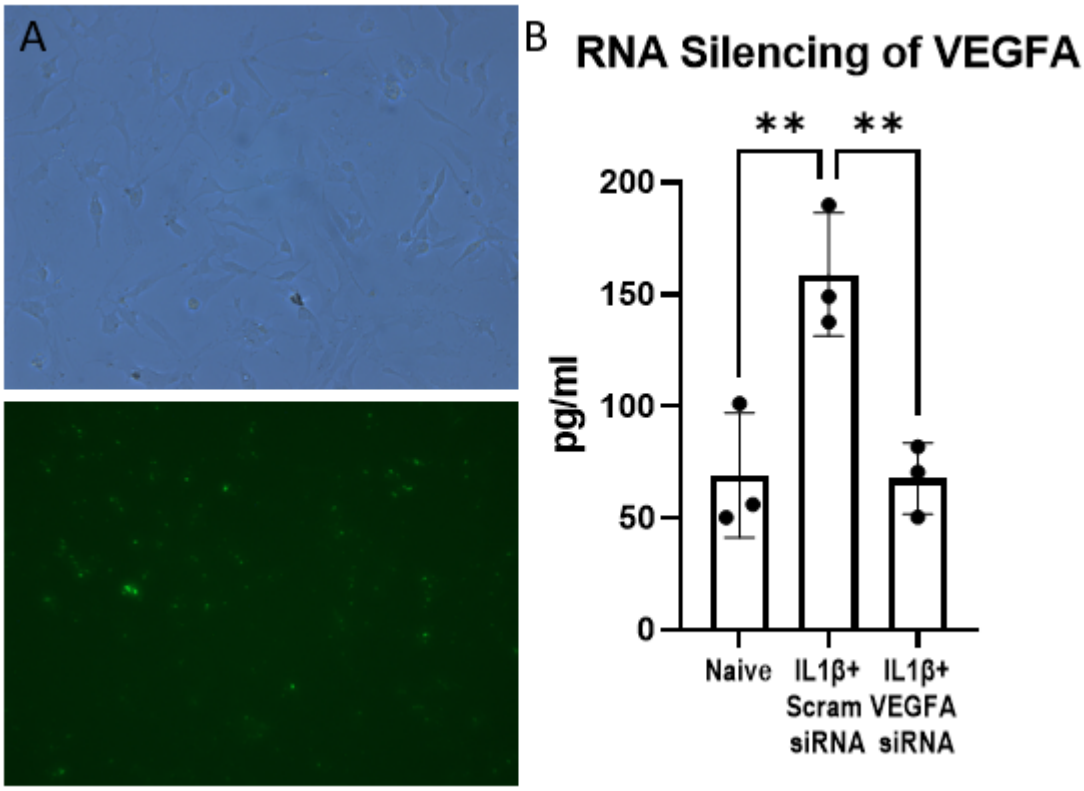

295

296 **Figure S8. Validation of VEGFA-siRNA Transfection in Disc Cells** A) Control siRNA (Fluorescein
297 Conjugate)-A revealed efficient transfection of cationic lipid-based transfection reagents in disc cells.
298 B) Stimulated disc cells by IL-1β with Scrambled siRNA shows a significant increase in the VEGF
299 secretion compared to naïve disc cells (158.9 ± 27.6 vs 69.1 ± 27.9, p=0.044). Stimulated disc cells with
300 IL-1β after being transfected with VEGFA siRNA showed a significant silencing (57.4%) of VEGFA
301 secretion compared to Scram siRNA (67.6 ± 16.0 vs 158.9 ± 27.6, p=0.034).

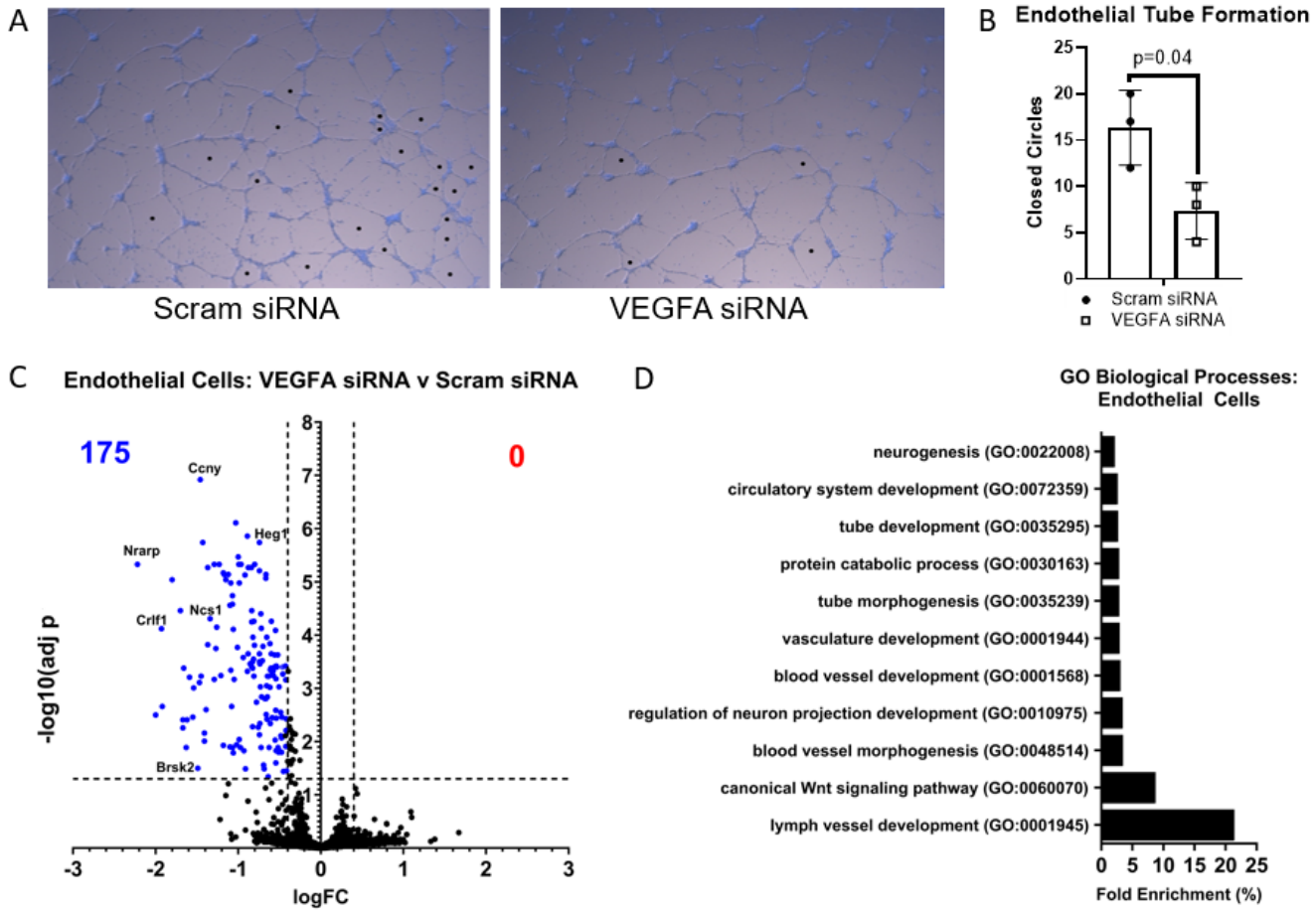

Fig. 7: VEGFA Inhibition Reduced *in vitro* Endothelial Cell Function and Regulates Gene Transcription A) Matrigel tube forming assay images of endothelial cells cocultured with human disc cells from degenerate discectomy tissue treated with siRNA showing initiation of vessel formation after 6 hours. B) VEGFA siRNA significantly reduced tube formation compared to Scrambled siRNA C) VEGFA siRNA regulated 176 differentially expressed genes. There is a suppression of key angiogenic genes including *Heg1*, *Narap*, and *Ncs1*. There is also a suppression of endothelial cell-derived neurogenic genes including *Brsk2* and *Crlf1*. D) The RNAseq analyses of the HMEC-1 also show that a ontological shift to lymphangiogenesism, matrix remodeling, and suppression of neurovascular regulating pathways.

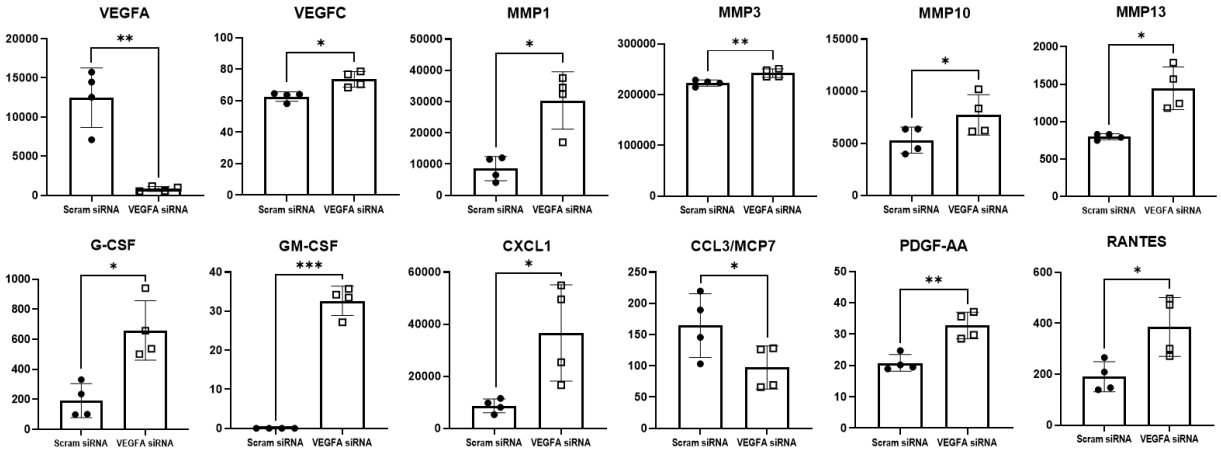

Fig. 8: The secreted factors from HMEC-1 (aka ECs) co-cultured with IVD cells were analyzed using the Luminex multiplex ELISA. Despite having a functional VEGFA gene, the ECs produced less VEGFA and CCL3 when co-cocultured VEGFA-silenced IL-1β–stimulated IVD cells. The ECs also produced more VEGFC and PDGF-AA that are both positive regulators of lymphangiogenesis; MMPs (MMP1, MMP3, MMP10, MMP13); chemokines including G-CSF, GM-CSF, CXCL1, and CCL5 (RANTES); and PDGF-AA, a positive relator of was also Units are pg/ml.

Group	Factor	Scrambled siRNA	VEGFA siRNA	p-value (paired)
Angiogenesis	Angiopoietin-2	29.1±2.1 (pg/ml)	28.9±2.4 (pg/ml)	0.53
Angiogenesis	Endoglin	84.8±10	92.9±5.9	0.06
Angiogenesis	Endothelin-1	337.3±42.5	336.7±34.9	0.84
Angiogenesis	Follistatin	436.8±485.1	915.9±1105.5	0.12
Angiogenesis	Leptin	70.4±11	70.4±8.4	0.79
Angiogenesis	PLGF	127.9±4	126.2±7.6	0.88
MMP	MMP2	8775±1081.8	9309.3±1816.7	0.55
MMP	MMP7	613.5±45.3	759.9±120.3	0.24
MMP	MMP8	138.6±116.4	239.4±120	0.30
MMP	MMP9	163±30.5	249.7±44.1	0.05
MMP	MMP12	582.4±65.1	604.9±59.9	0.60
MMP	TIMP1	100638.6±13530.7	89032.7±6718.9	0.13
MMP	TIMP2	30098.3±2192.1	31829.1±3278.2	0.07
MMP	TIMP3	3770.7±1298.2	2823.7±677.1	0.42
MMP	TIMP4	56.8±6.4	54.1±3.1	0.55
Cytokines	EGF	3.2±0.8	3.5±0.7	0.64
Cytokines	Eotaxin	7.7±0.6	7.6±0.7	0.89
Cytokines	FGF-2	187±72.4	200.5±58.4	0.23
Cytokines	FLT-3L	0.6±0.1	0.6±0.1	0.74
Cytokines	M-CSF	246.1±74.1	222.9±61	0.60
Cytokines	IL-6	2481.3±183	2518±201.4	0.94
Cytokines	IL-8	14958±894.4	16325.9±275.8	0.09
Cytokines	CCL2/MCP1	3441.9±1491.7	3898.9±1275.8	0.18
Cytokines	PDGF-BB	32.9±7.5	20.9±5.8	0.45

Supplemental Table 2**.** Panel of measured cytokines produced from the EC after co-culturing with the VEGFA-silenced IL-1β–stimulated IVD cells.

The factors secreted by endothelial cells co-cultured co-culturing with the VEGFA-silenced IL-1β-stimulated IVD cells reveals compensatory activity in the absence of VEGFA

After removal from the co-cultured conditions with the VEGFA-silenced, IL-1β-stimulated IVD cells, the HMEC-1 also secreted less VEGFA and CCL3, suggesting that the factors produced by the VEFA-silenced IVD cells contained less stimuli. Yet these HMEC-1s also produced more VEGFC, which is important for lymphangiogenesis; active matrix metalloproteinases (MMPs -1, -3, -10, and -13); G-CSF, GM-CSF, CXCL1, and CCL5 (RANTES) (Figure 8). The production of PDGF-AA suggests that there are compensation mechanisms to stimulate VEGFA. In all, IL-1β -stimulated IVD cells caused the HMEC-1s to form more mature tubular structures with more robust production of VEGFA. Silencing the VEGFA from these IVD cells prior to IL-1β -stimulation attenuated the tube formation

331 and resulted in reduced inflammatory factors but more MMPs, immune recruiting chemokines and
332 lymphoangiogenic factors, that indicates greater cellular emphasis on matrix remodeling and
333 lymphoangiogensis rather than angiogenesis. There are also a number of chemokines that are not
334 changed due to VEGFA-silencing of the IVD cells (Table S2).

335 **DISCUSSION**

336 This is the first study to demonstrate that intradiscal innervation contributes to locomotive performance
337 and pain sensitivity in a model of intervertebral disc degeneration. While many studies in the past have
338 shown progressive associations where neurovascular structures increase with progressive degeneration
339 and pain,[22-26] none have been able to block or prevent these structures to prevent chronic pain and
340 maintain locomotive performance. From this work, we also demonstrate that VEGFA may be a
341 therapeutic target for a disease modifying therapy of low back pain. While VEGFA ablation did not
342 significantly impact the structural and mechanical properties of the IVDs, it showed a pronounced effect
343 on neural and vascular infiltration and the subsequent mechanical sensitivity and locomotive
344 performance following degeneration.

345 VEGFA plays a crucial role in limiting nerve and vessel infiltration post-injury. IVD
346 degeneration in VEGFA-null mice exhibited significantly reduced neurite and vessel lengths and depths,
347 particularly in the outer annulus fibrosus (AF). VEGFA ablation inhibits the elongation and penetration
348 of neural and vascular structures in the normally avascular IVD, potentially preventing painful sensory
349 neurons from entering injured areas. The synergistic relationship between nerve and vessel infiltration
350 highlights VEGFA's importance in neurovascular coupling within the IVD, with its absence leading to
351 diminished neurite and vessel growth, which may limit painful neurological signals and affect overall
352 disc health. These findings emphasize VEGFA's critical role in supporting neural and vascular initiation
353 post-injury. Yet, the loss of VEGFA does not significantly influence IVD tissue degeneration, 3D
354 structure, or mechanical properties, and it is not a major contributor to structural or functional integrity
355 at the mechanical level during IVD degeneration.

356 The loss of VEGFA also appeared to reduce the neuropeptide-related signaling in TrKA,
357 TRPV1, and TRPA1 in the Dorsal Root Ganglion (DRG). The increase expression of these factors in

358 the DRG have been observed in chronic low back pain, as well as in DRG that are sensitive to capsaisin
359 stimulation. The decrease in TrKA activation could be responsible for the reduction in pain sensitivity
360 demonstrated by the Von Frey mechanical test. The results of the Von Frey mechanical test revealed
361 that VEGFA-null mice were less sensitive to pain than the wild-type mice. VEGFA removal also showed
362 a significant decrease in TRPA1 fluorescence, however, no cold sensitivity was observed. TRPV1 levels
363 did not have significant changes between VEGFA-null mice and wild-type mice. This data suggests that
364 there would be no observable difference in heat sensitivity between VEGFA-null mice and wild-type
365 mice, which is consistent with the hot plate experiment.

366 The behavioral assessments revealed that despite exhibiting acute pain post-injury, VEGFA-null
367 mice had improved recovery from mechanical sensitivity and avoided the chronic sensitivity observed
368 in WT mice. While VEGFA-null mice did not develop the performance impairments seen in WT mice
369 at later points (9-12 weeks), indicating a protective effect of VEGFA ablation against chronic pain and
370 impaired performance. Mechanical sensitivity showed imbalanced injury induced sensitivity while
371 VEGFA inhibition balanced this asymmetry demonstrating there is no global effect of pain alleviation,
372 and that VEGFA loss rescued the IVD injury effects but did not change systemic pain sensing.

373 *Elongation vs Sprouting*

374 Injuries to the intervertebral disc primarily trigger nerve and blood vessel sprouting as an adaptive
375 response to inflammation and hypoxia [27,28]. This sprouting—stimulated by factors like NGF and
376 inflammatory cytokines—leads to increased neurovascular infiltration into normally aneural and
377 avascular disc regions, contributing to chronic pain and ongoing inflammation.[29-31] Consistent with
378 these, we observed neurites and vessels infiltrating into the degenerating IVD at 3-weeks following the
379 injury. However, once sprouted, the neurites did not appear to elongate further, as evidenced by the
380 relative similar between the neurites between 3- and 12- weeks. In this animal model, VEGFA is

381 ubiquitously ablated from the whole animal, and it is not possible to determine the source of the VEGFA.
382 Our in vitro experiments however, support that blocking IVD-produced VEGFA was sufficient to
383 prevent growth of the neurites and the maturation of the blood vessels. RNAseq analysis suggest that
384 the reduced growth of neural outgrowths is driven suppression of cell proliferation. We observed similar
385 behavior in the endothelial cells, where the HMEC-1s co-cultured VEGFA-silenced IL-1β–stimulated
386 secreted VEGFC and PDGF-AA, both positive regulators of lymphangiogenesis, more MMPs, and more
387 immune cell recruiting chemokines. These immune cell recruiting chemokines are likely to be important
388 for the intrinsic healing of the IVD. [32] The RNAseq analyses of the HMEC-1 also show that a ontological
389 shift to lymphangiogenesism and matrix remodeling with a suppression of key angiogenic genes
390 including Heg1 Narap, and Ncs1. There is also a suppression of endothelial cell-derived neurogenic
391 genes including Brsk2 and Crlf1.

392 Needle stab injury models in animals are frequently utilized to study the pathophysiology of
393 intervertebral disc (IVD) degeneration and to develop treatments for chronic lower back pain (CLBP).
394 These models effectively replicate critical aspects of human disc degeneration, such as mechanical
395 damage, inflammatory responses, and biochemical changes. For example, they simulate the mechanical
396 damage caused by traumatic events and the inflammatory cytokine upregulation observed in human
397 discs, which are crucial for understanding the progression of disc degeneration.[33] However, these models
398 have limitations, especially in replicating the chronic, multifactorial nature of human CLBP and the
399 complexity of human pain perception.[34,35] Human IVD degeneration occurs over years and decades,
400 with the herniation of the IVD being one of the most apparent instigating factors. Despite the varied
401 etiologies of discogenic pain, the chronic symptoms and eventual degenerative presentation, such as the
402 deterioration of IVD structure, are quite similar. Therefore, the needle injury model in murine IVD is

403 employed to understand the mechanisms following IVD injury that eventually lead to low back pain
404 symptoms.

405 While these models are beneficial for basic research and initial therapeutic testing, their findings
406 must be interpreted with caution and validated in more complex models and ultimately in human clinical
407 studies. Differences in disc anatomy and biomechanics between humans and animals can affect the
408 translational relevance of these models, underscoring the need for complementary approaches to fully
409 capture the complexity of human IVD degeneration.[35] The needle injury in a mouse induces progressive,
410 but relatively rapid degeneration, occurring over weeks and months, compared to human degeneration,
411 which spans years and decades. Despite being traumatic relative to the human scale, this model is a
412 necessary caveat for developing feasible and mechanistic experiments. A single level lumbar injury
413 utilized here may also have underestimated the magnitude of our findings, since multiple groups have
414 shown a more pronounced pain behavior with 3 levels of injury in rodents. [36]

415 The multifactorial nature of the injury and VEGFA ablation at 3 weeks complicated the detection
416 of significant changes acutely, but by chronic timepoints, painful alterations were apparent.
417 Additionally, the WT sham group displayed elevated disc degeneration scores, suggesting that sham
418 procedures may induce a mild phenotype. Notably, neurovascular ingrowth was more pronounced on
419 the dorsal side opposite the ventral injury location, as seen by others,[22] likely due to its proximity to the
420 spinal cord and increased availability of neural and vascular sources. These findings are likely clinically
421 translatable as the treatment is compatible with the sequalae chronic low back pain development. Since
422 patients typically seek treatment only after an injury or an acute episode of pain, the timely post-injury
423 inhibition of VEGFA may be able to prevent the transition to chronic low back pain.

424 Overall, the loss of VEGFA appears to be protective against mechanical sensitivity, with
425 decreased innervation and no major impact on IVD degeneration. These findings, for the first time to

426 date, show a causative relationship between neurovascular pathoanatomy and pain while implicating
427 VEGFA as a critical mediator these processes following lumbar injury and highlight its potential as a
428 therapeutic target for preventing lower back pain through neurovascular inhibition. These findings are
429 likely clinically translatable as the treatment is compatible with the sequalae of chronic low back pain
430 development. Since patients typically seek treatment only after an injury or an acute episode of pain, the
431 timely post-injury inhibition of VEGFA may be able to prevent the transition to chronic low back pain.

432 **MATERIALS AND METHODS**

433 **Experimental Design**

434 *The Postnatal Inducible Ablation of VEGFA in Adult Mice*

435 Young adult, 4–6-month-old, ubiquitin (UBC)-Cre^{ERT2} ; VEGFA$^{fl/fl}$; Ai9 tomato reporter mice which
436 were previously described [37-39] were used on a C57BL/6J background and allow for a temporally
437 controllable ablation of VEGFA upon tamoxifen administration and report recombination via an Ai9
438 fluorescence reporter. This ubiquitous model systemically ablates VEGFA in all tissue. An estrogen
439 responsive Cre element is activated when a mutant estrogen receptor (ERT2) renders Cre active upon
440 tamoxifen binding and initiates a conformational change that allows Cre to enter the nucleus and catalyze
441 recombination at LoxP sites. These Cre+ mice allow for precise temporal control over gene
442 modification. Moreover, this approach can avoid developmental defects and embryonic lethality,
443 especially in pathways that are essential to organogenesis. All procedures (breeding, drug
444 administration, procedures, and tissue extraction) were performed with WUSM IACUC (Institutional
445 Animal Care and Use Committee) approval.

446

447 *Confirmation and Quantification of VEGFA Ablation*

448 The Ai9-tdTomato reporter protein is co-expressed with Cre recombinase presence, and it is visually
449 evident by inspection at the macroscopic scale after two doses of tamoxifen (100 mg/ kg) administered
450 over two consecutive days.

451 We also evaluated the efficiency of VEGFA ablation in the intervertebral disc by measuring the
452 production of the VEGFA protein secreted by the intervertebral disc (IVD). Mice with Cre- and Cre+
453 alleles driven by the ubiquitin promotor in animals with the homozygous VEGFA floxed alleles (UBC-

454 Cre^{ERT2}; VEGFA$^{fl/fl}$ Ai9) received 2 consecutive days of tamoxifen administration via oral gavage
455 (100 mg/kg in corn oil). The animals were sacrificed on the third day, following the two days of
456 induction. The functional spine units (FSUs), containing the vertebrae-intervertebral disc-vertebrae
457 structure were cultured as previously described and stimulated with TNFα (5ng/ml) to provoke an
458 inflammatory response.[40] Media was collected every other day for 7 days and analyzed using a VEGFA
459 ELISA (R&D Systems Cat: DY493).

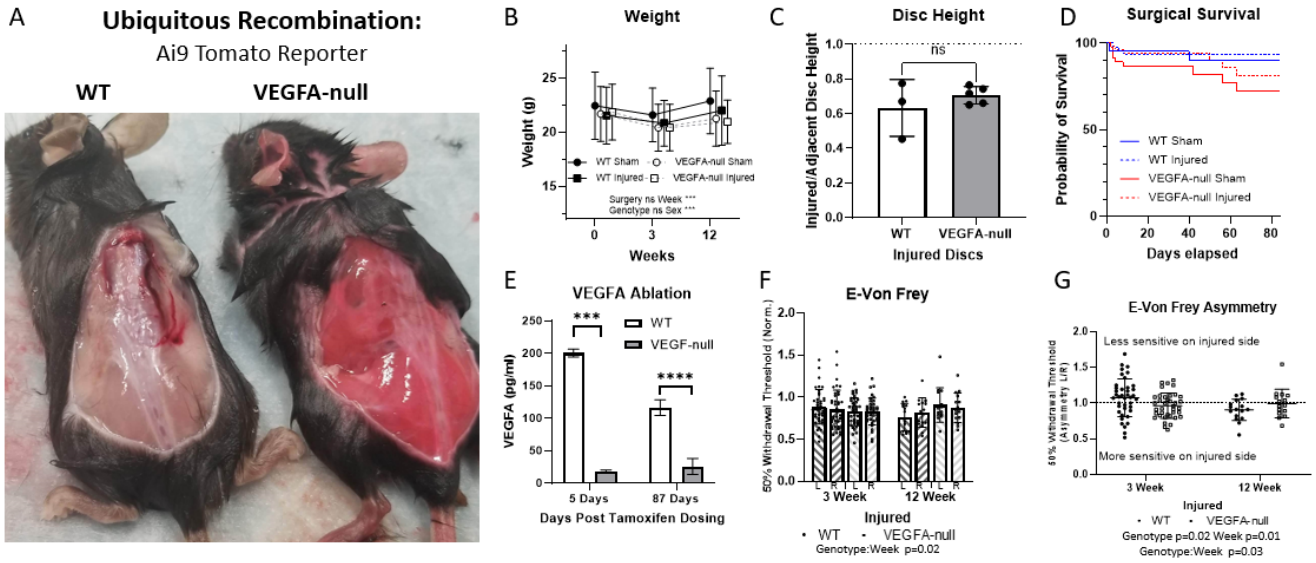

460

461 **Figure S2: Validation of VEGFA Ablation and Mouse Health** A) Ubiquitous recombination in a WT
462 and VEGFA-null showing the pink WT and red VEGFA-null Ai9 tdTomato reporter B) Mouse body
463 weights at 0 (Baseline), 3 and 12 weeks remain similar between groups irrespective of genotype or
464 surgery type C) Disc height ratio of injured/adjacent control disc height showing a similar decrease in
465 heights following injury D) Surgical survival curves show no significant differences between genotype
466 or surgery E) VEGFA ablation confirmation after initial ablation and 12 weeks from FSU media after
467 TNFα stimulation ELISA showing a sustained ablation over time F) E-Von Frey shows that WT injured
468 sensitivity increased over time (decreased withdrawal threshold) while VEGFA-null decreased over
469 time (increased withdrawal threshold) G) E-Von Frey asymmetry signifies an imbalance in WT mice

470 that fluctuates over time while VEGFA-null mice remained nearer to symmetry (dotted line). Data are
471 presented as mean ± standard deviation.

472 *The Lumbar Puncture Intervertebral Disc Injury Model*

473 Male and female mice of 4-6 months of age were randomly allocated into respective experimental
474 groups. The animals undergoing surgery were first anesthetized using a subcutaneous lidocaine injection
475 (0.5% at 7mg/kg) followed by isoflurane inhalation (3–4% v/v induction and 2–2.5% v/v maintenance
476 at 1 L/min flow rate). The left flank was shaved, and the skin sterilized with 70% ethanol and povidone
477 iodine. Under microscopic guidance, a retroperitoneal dissection was performed to expose the lateral
478 aspect of the spine using a Penfield dissector. The pelvis and hip were rotated posteriorly to enhance the
479 working space. The peritoneal wall was gently tugged to expose the psoas muscle, which was retracted
480 posteriorly to anteriorly using a cotton swab and then held in place with a metal spatula. The spinal
481 column and IVDs at the L5/6 and L6/S1 levels were exposed by blunt dissection. The superior margin
482 of the pelvic bone indicated the L6 vertebral body, confirming the locations of L5/6 and L6/S1 IVDs.
483 The L5/L6 IVD was targeted and either exposed in shams or injured with a 30G needle 3 times through
484 the annulus fibrosis and partially into the nucleus pulposus.[22,41]

485 Perioperatively, mice were monitored every 8–12 hours for 4 days post-surgery. Pain
486 management included intraperitoneal injections of carprofen (5 mg/kg) every 8–12 hours, supplemented
487 with carprofen tablets (2 mg/tablet) for 48-72 hours. On days 3 and 4 post-operatively, tamoxifen (TAM,
488 Cat#: T5648, Millipore Sigma) was given via oral gavage (100 mg/kg in corn oil, Cat#: C8267, Millipore
489 Sigma) to Cre+;VEGFA$^{fl/fl}$ animals (aka 'VEGFA-null') and Cre-;VEGFA$^{fl/fl}$ littermates ('WT')
490 inducing VEGFA ablation. Data collection occurred at 3 and 12 weeks with behavioral assays including
491 additional timepoints at baseline, within 7 days of injury, and longitudinal cohorts at 6 and 9 weeks.

492 Mouse weights were collected at baseline, 3, and 12 weeks to track overall health and survival was
493 tracked throughout the experiment to create Kaplan-Meier survival curves.

494 Acute 3-week post-op and chronic 12-week post-op time points were chosen with the acute
495 injury response allowing for the initial surgical wound healing recovery, while chronic LBP is defined
496 as pain lasting 12 weeks or longer.[42,43]

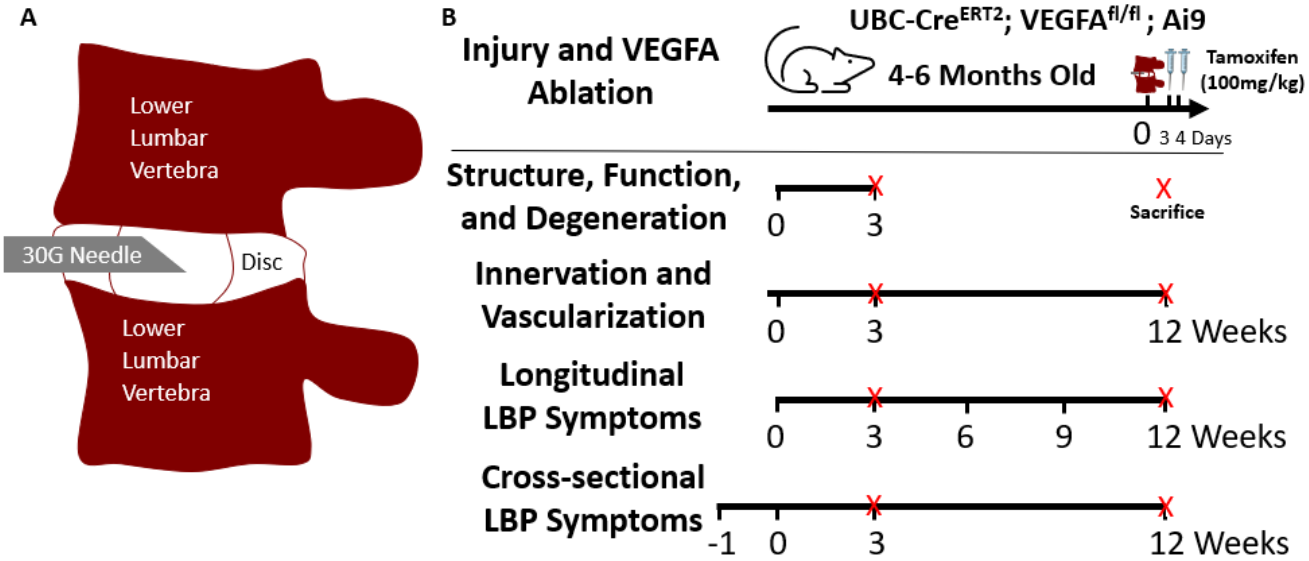

497

498 **Figure S1: Experimental Design** A) Lower lumbar disc puncture model showing the relative scale of
499 a 30G needle and the depth of injury B) Experimental design for various outcomes including injury at
500 time=0 with VEGFA ablation at 3-4 days Post-op, and acute and chronic terminal time points at 3 and
501 12 weeks. Baseline behavior within one week or surgery normalized behavioral outcomes.

502 **Histological analyses**

503 *Histopathological evaluation of degeneration*

504 To quantify acute IVD degeneration at 3 weeks, frozen 10 µm thick midsagittal sections were stained
505 with Safranin O / Fast Green and imaged at 10x on a Nanozoomer (Hamamatsu, Japan).
506 Histopathological scoring followed an established protocol for degeneration in four compartments of

507 the IVD including the NP, AF, end plate, and interface/boundary regions.[44] Mean degeneration scores
508 from three independent investigators (n=3/sex/genotype/surgery, N=24 total) were used for analysis.

509 *Structural quantification of Nerve and Vascular features by Immunohistochemistry*

510 Spines from the animals were fixed in 4% paraformaldehyde for approximately 48 hours, washed 6
511 times for 15 minutes each in 1X PBS, and subsequently demineralized in 14% EDTA for 10-14 days.
512 After which, samples were washed 8-10 times for 15 minutes in 1X PBS and serially infiltrated with
513 10%, 20%, and 30% sucrose solutions for 1 hour each prior to optimal cutting temperature (OCT)
514 infiltration and freezing for cryosectioning. Section thickness was 50 µm to provide a semi-3-
515 dimensional visualization of the neuronal and vascular morphology. Serial sections were collected with
516 CryoJane slides to adhere tissue to the slide during IHC staining with tissues being stored at -80°C prior
517 to antibody staining.

518

519 To stain for Protein Gene Product 9.5 (PGP9.5), Endomucin, and DAPI counter stain, a 4-day protocol[45]
520 was followed whereby slides were dried at room temperature for 30 minutes and washed in PBS 2 times
521 for 5 minutes. A PAP pen was used to create a hydrophobic perimeter around the tissue and allow for
522 direct pipetting of reagents onto the slides to avoid tissue loss from vertical slide immersion. Slides were
523 blocked with 10% donkey serum and 0.3% Triton X-100 in PBS for 1 hour at room temperature. The
524 primary PGP9.5 antibody (Millipore Cat # Ab1761) at a 1:1000 dilution and Endomucin antibody (Cat
525 #14-5851-85) at a 1:500 dilution was added to 1% normal donkey serum in a TNT (Tris-NaCl-Tween)
526 buffer and incubated 48 hours at 4°C in a humidified chamber. Samples were then washed 3 times for 5
527 minutes in TNT buffer prior to incubation of a PGP9.5 secondary antibody (Jackson Cat #711-545-152)
528 at 1:1000 concentration and 488nm fluorophore and Endomucin secondary antibody (Jackson Cat #712-
529 605-153) at 1:1000 concentration and 657nm fluorophore in 1% normal donkey serum in TNT buffer

530 for 24 hours at 4°C in a humidified chamber. Samples were washed 3 times with TNT for 5 minutes
531 prior to DAPI (Sigma-Aldrich D9542) at 1:1000 for 5 minutes at room temperature. A final wash with
532 TNT 3 times for 5 minutes was done prior to cover slipping and subsequent sealing of the slides with
533 Fluoromount-G a day later (Thermo Cat:00-4958-02).
534
535 To confirm that the PGP9.5 positive structures within the IVD are sensory neurons, we conducted a
536 direct comparison of the PGP9.5 straining of an injured intervertebral disc in a $Na_v1.8$ td tomato reporter
537 mouse and found the $Na_v1.8$+ features accounted for 88% of the PGP9.5+ features with a spatial
538 colocalization correlation of R=0.86. The sodium-sensitive ion channel $Na_v1.8$ is highly specific to
539 sensory neurons.[46-48] A serial section as described above was obtained and then stained for PGP9.5. We
540 then examined the localization and specificity of PGP9.5 and $Na_v1.8$ within the same section.
541
542 DAPI, PGP9.5, and Endomucin helped visualize, respectively, cell nuclei, broad neural populations, and
543 endothelial cells of vasculature via a confocal microscope (Leica, USA) at 2.5 μm focal depth in
544 increments with 10x magnification and 2048x2048 resolution and 600 speed with 2 frame averaging.
545 Excitation and emission wavelengths were set as follows: DAPI excitation 405nm and emission 414-
546 450 nm, PGP9.5 excitation 488nm and emission 498-530 nm, and Endomucin excitation 635nm and
547 emission 650-725 nm. Note that there was no overlap between the Ai9 tdTomato reported with excitation
548 of 554 and emission of 581nm. Neurite and vessel quantification of the outer AF were performed on
549 max projections of a Z-stack with Fiji (ImageJ), with lengths on or within the AF and the surrounding
550 fibrous tissue calculated from the Neuroanatomy SNT plugin and with depths calculated normal to the
551 peripheral edge of the AF. PGP9.5 staining showed some non-specific regions so was only not included
552 if neuronal morphology was apparent.

To quantify spatial coupling of neurites and vessels, an automated MATLAB was developed to measure lengths and depths and calculate colocalization lengths and a colocalization ratio based on distance from the rarer neurite features. Spatial coupling was defined as vessels within 30 µm from neurites and based on the distance between two adjacent lamellae as lamellar structure and proximity likely impact the transmission of neurovascular coupling signaling.

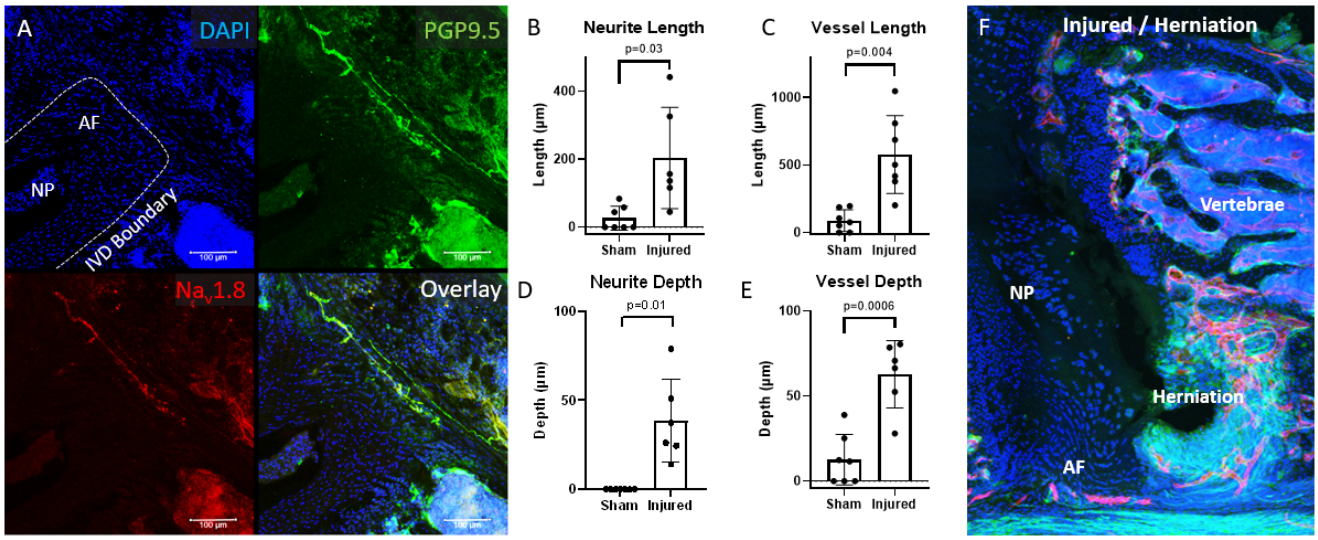

Figure S3: Validation of Neuronal Stain with Injury A) Validation of PGP9.5 IHC with a Na_v 1.8 showing the coincidence of the more specific sensory Na_v 1.8 with pan neuronal PGP9.5. B-E) Acute (3 week) neurite length and depth and vessel length and depth data showing the increased lengths associated with injured discs F) IHC of a herniated disc at 3 weeks showing diffuse non-specific green PGP9.5 staining and red Endomucin vessels. Data are presented as mean ± standard deviation.

Neuropeptide immunostaining of the Dorsal Root Ganglia

Frozen DRG sections were processed for immunohistochemistry using a standardized protocol across all targets. Briefly, slides were fixed in 4% paraformaldehyde for 10 minutes at room temperature. After washing in 0.1 M Tris buffer (pH 7.6), non-specific binding was minimized through sequential blocking

569 steps with 0.005% BSA in Tris and 10% normal goat serum. Sections were incubated overnight at 4°C
570 with primary antibodies—anti-TrkA (1:100, Alomone Labs #ANT-018), anti-TRPA1 (1:200, Alomone
571 Labs #ACC-037), or anti-TRPV1 (1:500, Abcam #ab6166)—diluted in Tris-BSA. After rinsing, a goat
572 anti-rabbit Alexa Fluor 488 secondary antibody (1:300, Invitrogen #A11006) was applied for 4 hours at
573 room temperature or overnight at 4°C. Nuclear counterstaining was performed using DAPI (1:5 dilution
574 in 0.1 M Tris), and slides were mounted prior to imaging. DRG immunohistochemical images were
575 quantified using the custom Python software, DRGVisual. Contrast Limited Adaptive Histogram
576 Equalization (CLAHE) was applied to enhance the contrast of the images. The processing began with
577 edge detection using Canny edge detection to refine the segmentation and ensure accurate depiction of
578 cell boundaries. Following edge detection, seed points within the cells were identified to indicate the
579 center of the cells, and diameters were drawn to estimate each cell's maximum size. Cell regions were
580 grown using a projection-based region-growing algorithm that expands the region from each seed point
581 by examining neighboring pixels and including them in the region if they meet criteria based on intensity
582 and connectivity. For each cell, the corrected total cell fluorescence (CTCF) was calculated by
583 subtracting the background intensity from each pixel's intensity within the cell region and summing the
584 total fluorescence across the cells for each ion channel.

585 **3D Structural Evaluation of Intervertebral Disc Structure Using µCT**

586 At 3 weeks post lumbar intervertebral disc injury, in vivo µCT was used to evaluate structural changes
587 of the intradiscal space (VivaCT, 45 kVp, 177 uA, 300 ms integration time, 10 µm voxel) with isoflurane
588 inhalation (2-3% v/v). Disc height was calculated in ImageJ as the average of 5 measures across the
589 midsagittal view.[41] To confirm that the loss of VEGFA did not affect the structure of the IVD, we
590 examined the uninjured L4-L5 and L6-S1 IVDs between the VEGFA KO and the WT animals.
591 Additionally, we examined the injured L5-L6 IVD level to ensure that the VEGFA KO animals were

592 susceptible to injury-mediated degeneration. An independent 2-tailed t-test was used to determine
593 differences between groups.
594
595 The structural changes at this 3-week post injury time point were further evaluated using the e*x vivo*
596 contrast-enhanced micro-computed tomography (CEμCT). Ioversol as the contrast agent was used to
597 highlight the water-rich nucleus pulposus.[49] The fresh IVDs were immersed in 50% ioversol (OptiRay
598 350, Guerbet Pharma) at 37°C for 24 hours before imaging. The Scanco40 μCT system (Zurich,
599 Switzerland) scanned samples at 45 keVp, 177 μA, 10.5 μm voxel size, and 300 ms integration after the
600 incubation[50]. Groups were n=3 mice/sex/genotype/injury. Total disc ROI and nucleus pulposus ROI
601 were contoured using the MATLAB graphical user interface from Washington University
602 Musculoskeletal Image Analyses (github.com). NP hydration, a ratio of nucleus attenuation to total disc
603 attenuation (NI/DI), was calculated along with volumes and disc height index, DHI, as an average of 5
604 height measures in a midsagittal slice over the disc width.
605
606 **Biomechanical Assessment of the Intervertebral Disc**
607 Mechanical behavior of the IVDs using dynamic compression testing under displacement control was
608 conducted using a BioDent reference point indenter (Active Life Scientific).[51] After CEuCT, these
609 samples (n=3 mice/sex/genotype/injury) were mechanically tested with the strain rate calculated from
610 the 5-point average disc height. FSUs were affixed to aluminum platens and immersed in a phosphate-
611 buffered saline bath at room temperature and preloaded to 0.25N. A sinusoidal compressive waveform
612 at 10% strain and 1 Hz frequency was applied for 20 cycles. The average stiffness was calculated from
613 the second through the final loading cycles and the loss tangent, or dissipation factor, was calculated
614 from the phase angle between load and displacement data.

615 **Behavioral Assessments**

616 Habituation measures were taken to reduce animal stress. Acclimation to room environment prior to
617 behavioral assessment was set for 1 hour at the beginning of each behavioral testing week. To avoid
618 additional animal stress, assessments were typically performed twice a day with 1 hour rest between
619 tests between 9am-5pm to minimize the effect of activity changes due to diurnal variations.[52] All tests
620 were performed by the same laboratory personnel. Baseline data was collected one week prior to surgery
621 and post-operative data collection included a cross-sectional group at baseline, 3, and 12 weeks and a
622 longitudinal group at 3, 6, 9, and 12 weeks. Care was taken to ensure a clean and odor-free environment.
623 The procedures were conducted in a quiet room with controlled temperature (20-23°C). Testing was
624 initiated up to one week prior to the 3- and 12-week time points as the full set of assays took 4-5 days
625 to complete with efforts made to reproduce the order and timing of each test to remove stress on the
626 animals and replicate methods.

627 *Mechanical Sensitivity measured using the Von Frey and E-Von Frey*

628 Mechanical sensitivity was measured using the up-down method of the Von Frey test using Semmes
629 Weinstein filaments (Bioseb, France) and an electronic Von Frey (Figure 2-6C, EVF, BIOSEB,
630 France).[53,54] Prior to baseline behavioral testing, mice were habituated to the elevated mesh grid chamber
631 for 1 hr. Calibrated filaments were applied to the plantar surface (Figure 2-5D) of the hind paw to elicit
632 paw withdrawal or filament buckling.[55] Filament Von Frey was done on the left hind paw to focus on
633 the injury response. EVF consisted of maximum force values at withdrawal from the median of the result
634 of 3 trials which were conducted bilaterally, with at least 5 min between testing opposite paws, and at
635 least 10 min between testing the same paw. Post-op measures were normalized to baseline.

636

637 *Hot and Cold Nociceptive Sensitivity*

638 Mice were subjected to thermal stimulus to measure the temperature sensitivity response.[56,57] A hot/cold
639 plate (Bioseb, France) was set to 55±0.5°C or 5±0.5°C and mice were placed individually onto the plate
640 with a transparent cylinder to prevent escape and allow for visibility. The latency to the first sign of
641 nociceptive behavior, either lick of the hand paws or jumping for hot plate and lifting, licking, or shaking
642 of the hind paws for cold plate was recorded with a cutoff time of 20 seconds for hot or 30 seconds for
643 cold to prevent tissue damage. Three repeated measures were collected with >15 minutes between tests
644 to allow for home cage recovery. Values were averaged and normalized to baseline.

645 Functional Assessments of Performance

646 *Locomotor Function – Rotarod*

647 Assessing motor coordination and balance, the Rotarod performance test challenged mice to a rotating
648 rod apparatus (Bioseb, France).[54,58,59] Prior to testing, mice were trained on the Rotarod at a slow 4 rpm
649 for 2 minutes to ensure baseline capabilities. Mice unable to achieve this baseline capacity were
650 excluded from assessment. On a subsequent day, mice were tested on an accelerating bar from 4 to 40
651 rpm over a 2-minute period. Latency to fall was recorded for each mouse. Each mouse underwent 5
652 trials with a >5-minute rest period between trials to reduce fatigue. The best performance of the 5 trials
653 was used for data analysis and normalized to baseline when possible.

654 *Open Field Testing*

655 In the open field test designed to evaluate exploratory passive behavior, mice were individually
656 introduced into the center of an open field arena (40 cm x 40 cm, with 30 cm high walls) equipped with
657 an automated tracking system (Omnitech Electronics, Columbus, OH).[54,58,59] The apparatus featured an
658 array of infrared sensors for precise movement tracking over a 60-minute test period. Behavioral
659 parameters recorded included total distance traveled and instances of vertical rearing, among others.

660 Between tests, the arena was cleaned with Cavicide and water to disinfect and eliminate residual odors
661 and waste. The total distance and rearing events were reported over 60 minutes.

662 Strength

663 *Inverted wire hang endurance*

664 In the wire hang behavioral test, mice were evaluated for neuromuscular strength and endurance.[60] The
665 apparatus consisted of a wire mesh (2 mm diameter) suspended above a soft bedding layer to ensure a
666 safe landing for the mice. Each mouse was gently held by the base of the tail and allowed to grasp the
667 wire at a 60° incline before the mesh was inverted to 180°. The duration the mouse remained suspended
668 inverted was recorded up to a maximum of 2 minutes. A minimum 5-minute rest was given between
669 trails. The maximum time of three trials was recorded.

670

671 *Grip Strength*

672 Grip strength, a measure of neuromuscular strength, was measured using a uniaxial grip force tester
673 (Bioseb, France).[61] Hind paw grip strength assessed mechanical strength as the mouse was gently
674 restrained and allowed to freely grab and hold a bar with both hind paws. Maximum force was recorded
675 as the tail was pulled in a consistent manner to avoid rate-dependent effects. A brief rest period, >15
676 sec, was given between each of the 5 repeated trials. Average strength was reported normalized to body
677 weight at the time of testing and normalized to baseline.

678 **Cell Culture**

679 *Human primary IVD Cell Culture*

680 Human intervertebral disc cells were isolated from the disc tissue of eight patients (mean age ± SD =
681 68.5 ± 8.1; female:male = 5:3; mean Pfirrmann grade ± SD = 3.5 ± 0.7) removed during elective
682 discectomy surgeries (Supplemental Table 5). Human biospecimens were obtained under IRB

683 Exemption Category 4, in accordance with institutional and federal guidelines for research using de-
684 identified, previously collected samples, as exemplified in prior studies (PMC7608136) and
685 (PMC5536110). Tissue specimens were placed in sterile Ham's F-12 medium (F-12; Gibco-BRL,
686 Grand Island, NY) containing 1% penicillin/streptomycin (P/S; Gibco-BRL) and 5% fetal bovine
687 serum (FBS; Gibco-BRL). Disc tissue was washed three times with Hank's balance salt solution
688 (HBSS; Gibco-BRL) containing 1% P/S to remove blood and other bodily contaminants prior to
689 isolation. Specimens were minced and digested for 60 min at 37°C under gentle agitation in F-12
690 medium containing 1% P/S, 5% FBS, and 0.2% pronase (Calbiochem, La Jolla, CA). The specimens
691 were rinsed three times with HBSS and 1% P/S and incubated overnight in a solution of F-12 medium
692 containing 1% P/S, 5% FBS, and 0.025% collagenase I (Sigma Chemical Co, St. Louis, MO). A sterile
693 nylon mesh filter (70 µm pore size) was used to separate suspended cells from the remaining tissue
694 debris. Isolated cells were centrifuged (2000 rpm, 5 min) and resuspended in F-12 medium with 10%
695 FBS and 1% P/S. Cells were plated in a 75-cm^2 culture flask (VWR Scientific Products, Bridgeport,
696 NJ) and incubated at 37°C, 5% CO^2, 20% O^2 in a humidified incubator. Culture medium was changed
697 three times weekly, and cultures grew to 90% confluence. Cells were then trypsinized (0.05%
698 trypsin/ethylene diaminetetraacetic acid; Gibco-BRL) and re-plated (6 x 10^5 cells/mL) in 75-cm^2
699 culture flasks.

Age	Sex	T12/L1	L1/2	L2/3	L3/4	L4/5	L5/S1	Mean	STD	Endothelial Cell (RNA/ multiplex/ ELISA)	Matrigel Outgrowth Assays	with Neural Cell (RNA/neurite)
70	F		3	3	4	4	4	3.6	0.5		X	
73	F			3	3	4	5	3.8	1.0	X		
73	M			3	3	3	4	3.3	0.5			X
66	F	3	3	3	5	5		3.8	1.1	X	X	
50	M					3	4	3.5	0.7	X		
76	F		2	3	3	4		3.0	0.8			X
68	F					3	3	3.0	0.0			X
72	M	3	3	4	4	4	5	3.8	0.8		X	

Table S5: Patients' Demographics for Disc Cells (DCs): DCs were isolated from the disc tissue of eight patients removed during elective surgical procedures for degenerative spinal disease. Phirman Grades for T12/S1 are shown along with assay distributions for each patient sample.

Immortalized human microvascular endothelial cell (HMEC-1) culture

HMEC-1(CRL-3243; ATCC, Masassas, VA) were cultured in MCDB 131 medium (10372019; Gibco-BRL) containing 10 ng/mL epidermal growth factor (PHG0311; Thermo Fisher Scientific, Waltham, MA), 500 mg/mL hydrocortisone (H0396; Sigma), 1% P/S, 2 mM L-Glutamine and supplemented with 10% FBS. Cells at passage number 5-10 were plated at 75 cm^2 culture flask and grown to 90% confluence.

Immortalized human neuroblastoma cell (SH-SY5Y) culture

The SH-SY5Y human neuroblastoma cell line (CRL-2266; ATCC) was cultured in a 1:1 mixture of Eagle's Minimum Essential Medium (EMEM; ATCC, Manassas, VA) and Ham's F12 medium, supplemented with 10% FBS and 1% P/S in a 5% carbon dioxide humidified incubator at 37°C. Cells at passage number 5-10 were plated at 75 cm^2 culture flask and grown to 90% confluence.

714 *Vascular Endothelial Growth Factor (VEGF)-siRNA Transfection*

715 Isolated human IVD cells were seeded in 6-well plates at a density of $3x10^5$ cells per well 24 hours prior
716 to transfection. VEGF-specific siRNA (sc-29620; Santa Cruz Biotechnology, Dallas, Tx) and scrambled
717 control siRNA- FITC (sc-36869; Santa Cruz Biotechnology) were transfected into DCs using
718 Lipofectamine™ RNAiMAX Transfection Reagent (Catalog #: 13778100, Thermo Fisher) following
719 the manufacturer's protocol. The final concentration of siRNA in the culture medium was 50 pM. The
720 effectiveness of transfection was evaluated by checking the amount of the secreted VEGF in media using
721 ELISA (DY293; R&D system, Minneapolis, MN) and confirming transfection of control siRNA by
722 FITC fluorescence with a Nikon Eclipse Ti2 inverted scope at 10x.

723 *Co-culture between IVD cells and HMEC-1 (ECs) Cells*

724 IVD cells were plated in a 6 well plate and transfected with either control, scrambled siRNA (Scram
725 siRNA) or with VEGF specific siRNA (VEGF siRNA). Medium with 1% FBS and recombinant human
726 interleukin-1β (IL-1β; R&D Systems) at 1 ng/mL was added to stimulate Scram siRNA (IL-1β+Scram
727 siRNA) and VEGF siRNA (IL-1β+VEGF siRNA) transfected IVD cells for 24 hours. After stimulation,
728 HMEC-1 cells "ECs" that were plated for 24 hours on 1 μm pore co-culture inserts (Thincert cell culture
729 insert; Greiner, Monroe, NC) at a density of $3x10^5$ cells were inserted to the wells containing Scram
730 siRNA or VEGF siRNA transfected IVD cells with MCDB media plus 1% FBS. ECs co-cultured with
731 stimulated Scram siRNA treated IVD cells are denoted as $EC_{IL\text{-}1\beta+Scram\ siRNA}$ and ECs co-cultured
732 stimulated with VEGF siRNA treated IVD cells are denoted as $EC_{IL\text{-}1\beta+VEGF\ siRNA.}$ Naïve ECs that did
733 not undergo co-culturing were used as a control group. ECs were analyzed via a Matrigel tube formation
734 assay, multiplex, and RNA sequencing. (Supplement Figure 6)

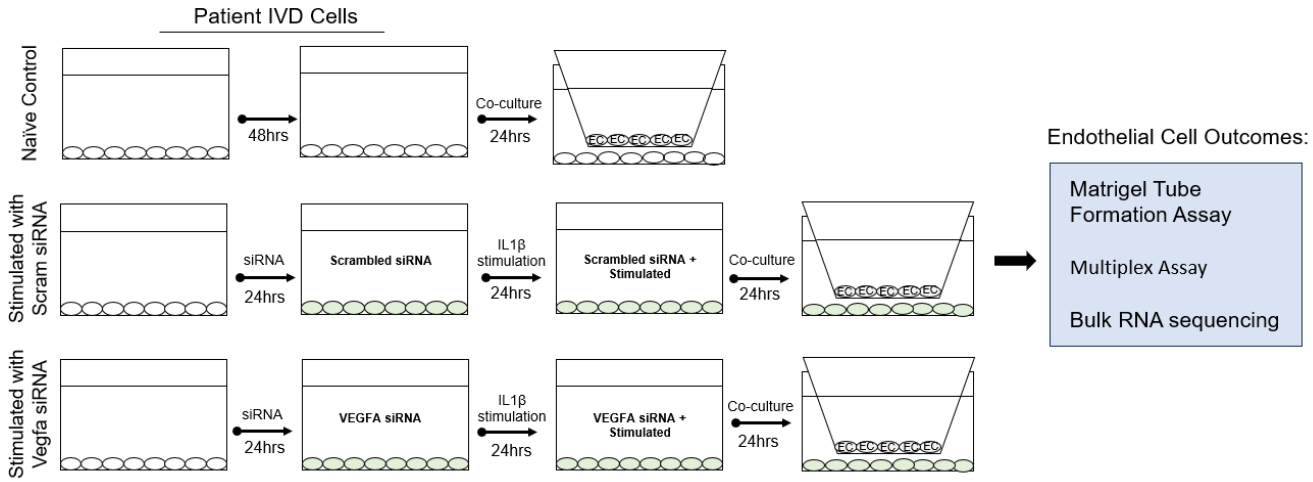

Figure S6. Schematic drawing of Co-culture between Disc Cells (DCs) and HMEC-1(ECs). DCs were plated on a 6 well plate left as naïve or transfected with Scrambled control siRNA (Scram siRNA) or VEGFA specific siRNA (VEGFA siRNA) for 24 hours. Cells were then treated with 1 ng/mL of IL-1β to stimulate the Scram siRNA and VEGF siRNA transfected DCs (IL-1β+Scram siRNA or siRNA IL-1β+VEGF siRNA, respectively) for 24 hours but the naïve DCs were left unstimulated. After stimulation, 1 µm pore co-culture inserts plated with ECs were inserted into each well for direct coculturing for 24 hours.

Co-culture between IVD cells and SH-SY5Y Cells (NCs)

SH-SY5Y neuronal cells "NCs" were plated at a density of 1.5 x 10^5 cells per well in a 6 well plate and cultured for 48 hours prior to co-culture experiment. For co-culturing, non-stimulated IVD cells "naive", IL-1β+Scram siRNA, and IL-1β+VEGF siRNA transfected IVD cells were plated on the co-culture insert at a density of 3.0 x 10^5 cells and co-cultured for 48 hours with NCs. NCs were analyzed via a neurite outgrowth assay and RNA sequencing. (Supplement Figure S7)

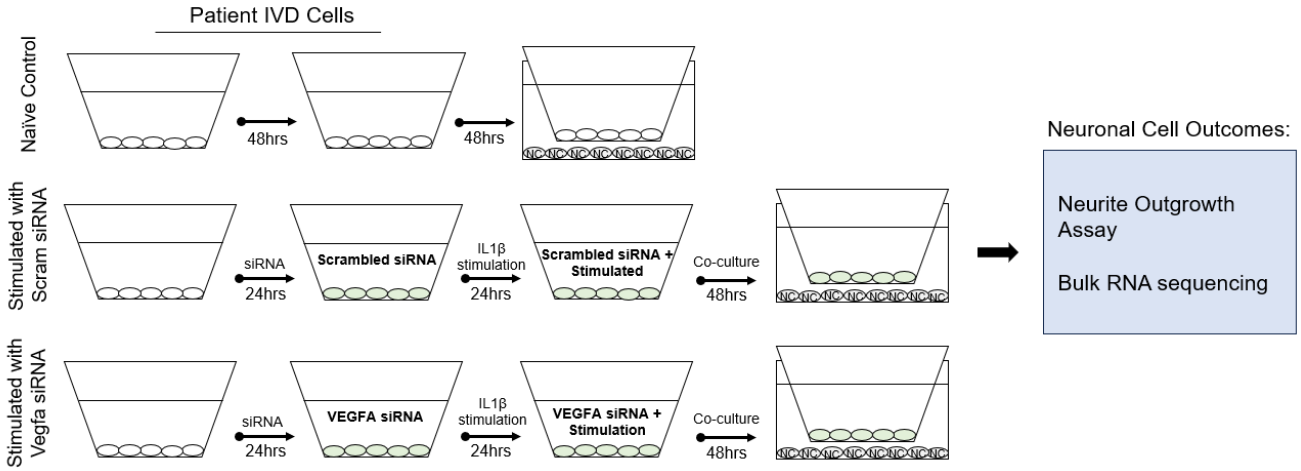

Figure S7. Schematic drawing of Co-culture between Disc Cells (DCs) and SH SY5Y cells (NCs). NCs were plated on a 6 well plate and cocultured with 1 μm pore co-culture inserts plated with DCs 48 hours. DCs were either left as naïve or transfected with Scrambled control siRNA (Scram siRNA) or VEGFA specific siRNA (VEGFA siRNA) for 24 hours. The naïve DCs were left unstimulated and the Scram siRNA and VEGF siRNA transfected DCs were stimulated with 1 ng/mL of IL-1β (IL-1β+Scram siRNA or siRNA IL-1β+VEGF siRNA, respectively) for 24 hours before coculturing.

RNA Sequencing and Gene Ontology

Post co-culture experiments, HMEC-1 and SH-SY5Y cells were lysed (TRIzol reagent, Fisher Scientific), and total RNA was extracted (Direct-zol RNA MicroPrep Kit, Zymo Research). Samples were prepared according to library kit manufacturer's protocol, indexed, pooled, and sequenced on an Illumina NovaSeq X Plus. Basecalls and demultiplexing were performed with Illumina's DRAGEN and BCLconvert version 4.2.4 software. RNA-seq reads were then aligned to the Ensembl release 101 primary assembly with STAR version 2.7.9a1. Gene counts were derived from the number of uniquely aligned unambiguous reads by Subread:featureCount version 2.0.32. Isoform expression of known Ensembl transcripts were quantified with Salmon version 1.5.23. Sequencing performance was assessed for the total number of aligned reads, total number of uniquely aligned reads, and features detected. The

768 ribosomal fraction, known junction saturation, and read distribution over known gene models were
769 quantified with RSeQC version 4.04. All gene counts were then imported into the R/Bioconductor
770 package EdgeR5 and TMM normalization size factors were calculated to adjust for samples for
771 differences in library size. Ribosomal genes and genes not expressed in the smallest group size minus
772 one sample greater than one count-per-million were excluded from further analysis. The TMM size
773 factors and the matrix of counts were then imported into the R/Bioconductor package Limma6.
774 Weighted likelihoods based on the observed mean-variance relationship of every gene and sample were
775 then calculated for all samples and the count matrix was transformed to moderated log 2 counts-per-
776 million with Limma's voomWithQualityWeights7. The performance of all genes was assessed with
777 plots of the residual standard deviation of every gene to their average log-count with a robustly fitted
778 trend line of the residuals. Differential expression analysis was then performed to analyze differences
779 between conditions and the results were filtered for only those genes with Benjamini-Hochberg false-
780 discovery rate adjusted p-values less than or equal to 0.05. The raw data files are available on the Gene
781 Expression Omnibus database: GSE294577

782 For gene ontology analyses, biological pathways enriched by the upregulated and downregulated
783 DEGs were identified by using the Panther Classification System with version Panther 19.0 by using
784 the statistical overrepresentation test. For endothelial cells, an adjusted p value of $p < 0.05$ and logFC
785 of 0.41 was used to identify statistically significant DEGs with at least a 50% increase in fold change of
786 the treatment group when compared to the control. For neuronal cells, an adjusted p value of $p < 0.10$
787 and logFC of 0.41 was used to identify statistically significant DEGs with at least a 50% increase in fold
788 change of the treatment group when compared to the controls. The full list of all GO terms for the
789 endothelial cells comparisons are listed in Supplemental Tables X' and X' and for the neuronal cell
790 comparisons are listed in Supplemental Tables X and X.

791 *Multiplex Protein Assay*

792 The supernatant from naive ECs and those co-cultured with IL-1β+Scram siRNA and IL-1β+VEGF
793 siRNA transfected IVD cells was collected and analyzed by multiplex protein assay (Human
794 Angiogenesis & Growth Factor 17-Plex, Human Cytokine Panel A 48-Plex, Human MMPTIMP 13-
795 Plex, Eve Technologies, Calgary, Alberta, Canada). Out of range values or results < 2pg/ml were not
796 included.

797

798 *Matrigel Tube Formation Assay*

799 To determine the vessel formation capacity between ECs cultured with conditioned media (CM)
800 collected from IL-1β+Scram siRNA versus IL-1β+VEGF siRNA transfected IVD cells, a Matrigel tube
801 formation assay was performed. Matrigel matrix (356231; Corning Inc., Corning, NY), a gelatinous
802 protein mixture that mimics the extracellular matrix, was used to coat a 24-well plate following the
803 manufacturer's protocol. HMEC-1 cells at the density of 3×10^4 cells per well were suspended in the
804 CM collected from IL-1β+Scram siRNA or IL-1β+VEGF siRNA transfected IVD cells for 48 hours and
805 plated onto each Matrigel coated well. Images were acquired at 6 hours and 12 hours post plating via a
806 Nikon Eclipse Ti2 inverted scope at 10x. To assess the ability of tube formation by each conditioned
807 media and time point, the numbers of closed loops were counted.[62]

808

809 *Neurite Outgrowth Assay*

810 The number and length of neurites from NCs co-cultured with non-stimulated IVD cells "naive", IL-
811 1β+Scram siRNA, or IL-1β+VEGF siRNA transfected IVD cells were compared. Neurite outgrowth
812 was quantified using ImageJ software. For each neuron, neurite number and length was counted
813 manually. Neurite length was measured from the edge of the cell body to the tip of the neurite. The

814 average neurite length per neurite was calculated for each treatment group, with all measurements
815 expressed in microns.

816

817 **Statistical Analysis**

818 Statistical comparisons on repeated measures, IE longitudinal behavioral assays, were done using a
819 linear mixed effect model to assess surgery (Sham/Injured), genotype (WT/VEGFA-null), weeks after
820 surgery (3/12), sex (M/F), and surgery (Naïve/Sham). Linear mixed effect models were initiated with
821 all factors and reduced in complexity as factors were found to be not significant. Additionally, focused
822 questions were modeled to assess injured groups with genotype and week. A 2 or 3 factor ANOVA was
823 used on terminal measures such as Ex Vivo CEμCT, biomechanics, disc degeneration scoring, or
824 immunohistochemistry to assess effects of injury, genotype, and sex. ANOVA pairwise comparisons
825 were done with the Fisher's Least Significant Difference method. Survival curves implemented Mantel-
826 Cox test while binary penetration results used a Fisher's exact test. Simple pairwise comparisons were
827 done using a Welch's t-test when appropriate. Appropriate adjustments were made in the respective
828 statistical models for unequal variances and non-normal distributions. The ROUT outlier test with
829 Q=0.1% removed definitive outliers within groups.[63] R and GraphPad Prism were used to model results.

REFERENCES

1. Airaksinen O, Brox JI, Cedraschi C, et al. Chapter 4. European guidelines for the management of chronic nonspecific low back pain. *Eur Spine J*. Mar 2006;15 Suppl 2(Suppl 2):S192-300. doi:10.1007/s00586-006-1072-1
2. Hartvigsen J, Hancock MJ, Kongsted A, et al. What low back pain is and why we need to pay attention. *Lancet*. Jun 9 2018;391(10137):2356-2367. doi:10.1016/S0140-6736(18)30480-X
3. Yang H, Haldeman S. Behavior-Related Factors Associated With Low Back Pain in the US Adult Population. *Spine (Phila Pa 1976)*. Jan 1 2018;43(1):28-34. doi:10.1097/BRS.0000000000001665
4. Shokri P, Zahmatyar M, Falah Tafti M, et al. Non-spinal low back pain: Global epidemiology, trends, and risk factors. *Health Sci Rep*. Sep 2023;6(9):e1533. doi:10.1002/hsr2.1533
5. Hoy D, March L, Brooks P, et al. The global burden of low back pain: estimates from the Global Burden of Disease 2010 study. *Ann Rheum Dis*. Jun 2014;73(6):968-74. doi:10.1136/annrheumdis-2013-204428
6. Collaborators GBDLBP. Global, regional, and national burden of low back pain, 1990-2020, its attributable risk factors, and projections to 2050: a systematic analysis of the Global Burden of Disease Study 2021. *Lancet Rheumatol*. Jun 2023;5(6):e316-e329. doi:10.1016/S2665-9913(23)00098-X
7. Rannou F, Lee TS, Zhou RH, et al. Intervertebral disc degeneration: the role of the mitochondrial pathway in annulus fibrosus cell apoptosis induced by overload. *Am J Pathol*. Mar 2004;164(3):915-24. doi:10.1016/S0002-9440(10)63179-3
8. Feng Y, Egan B, Wang J. Genetic Factors in Intervertebral Disc Degeneration. *Genes Dis*. Sep 2016;3(3):178-185. doi:10.1016/j.gendis.2016.04.005
9. Wang F, Cai F, Shi R, Wang XH, Wu XT. Aging and age related stresses: a senescence mechanism of intervertebral disc degeneration. *Osteoarthritis Cartilage*. Mar 2016;24(3):398-408. doi:10.1016/j.joca.2015.09.019
10. Luoma K, Riihimäki H, Luukkonen R, Raininko R, Viikari-Juntura E, Lamminen A. Low Back Pain in Relation to Lumbar Disc Degeneration:. *Spine*. 02/2000 2000;25(4):487-492. doi:10.1097/00007632-200002150-00016
11. Urban JP. Swelling pressure of the lumbar intervertebral discs: influence of age, spinal level, composition, and degeneration. *Spine*. Feb 01 1988;13(2):179-187.
12. Buckwalter JA. Aging and degeneration of the human intervertebral disc. *Spine (Phila Pa 1976)*. Jun 1 1995;20(11):1307-14. doi:10.1097/00007632-199506000-00022
13. Adams MA, Freeman BJ, Morrison HP, Nelson IW, Dolan P. Mechanical initiation of intervertebral disc degeneration. *Spine (Phila Pa 1976)*. Jul 1 2000;25(13):1625-36. doi:10.1097/00007632-200007010-00005
14. Setton LA, Chen J. Mechanobiology of the intervertebral disc and relevance to disc degeneration. *The Journal of Bone and Joint Surgery American Volume*. 2006-04 2006;88 Suppl 2:52-57. doi:10.2106/JBJS.F.00001
15. Binch ALA, Fitzgerald JC, Growney EA, Barry F. Cell-based strategies for IVD repair: clinical progress and translational obstacles. *Nat Rev Rheumatol*. Mar 2021;17(3):158-175. doi:10.1038/s41584-020-00568-w
16. Binch ALA, Cole AA, Breakwell LM, et al. Nerves are more abundant than blood vessels in the degenerate human intervertebral disc. *Arthritis Research & Therapy*. 12/2015 2015;17(1)doi:10.1186/s13075-015-0889-6

17. Sato J, Inage K, Miyagi M, et al. Inhibiting Vascular Endothelial Growth Factor in Injured Intervertebral Discs Attenuates Pain-Related Neuropeptide Expression in Dorsal Root Ganglia in Rats. *Asian spine journal*. Aug 2017;11(4):556-561. doi:10.4184/asj.2017.11.4.556

18. Carmeliet P, Ruiz de Almodovar C. VEGF ligands and receptors: implications in neurodevelopment and neurodegeneration. *Cell Mol Life Sci*. May 2013;70(10):1763-78. doi:10.1007/s00018-013-1283-7

19. Falk T, Gonzalez RT, Sherman SJ. The yin and yang of VEGF and PEDF: multifaceted neurotrophic factors and their potential in the treatment of Parkinson's Disease. *Int J Mol Sci*. Aug 5 2010;11(8):2875-900. doi:10.3390/ijms11082875

20. Rickman M, Ghim M, Pang K, et al. Disturbed flow increases endothelial inflammation and permeability via a Frizzled-4-beta-catenin-dependent pathway. *J Cell Sci*. Mar 15 2023;136(6)doi:10.1242/jcs.260449

21. Dejana E. The role of wnt signaling in physiological and pathological angiogenesis. *Circ Res*. Oct 15 2010;107(8):943-52. doi:10.1161/CIRCRESAHA.110.223750

22. Lee S, Millecamps M, Foster DZ, Stone LS. Long-term histological analysis of innervation and macrophage infiltration in a mouse model of intervertebral disc injury-induced low back pain. *J Orthop Res*. Jun 2020;38(6):1238-1247. doi:10.1002/jor.24560

23. Freemont AJ, Peacock TE, Goupille P, Hoyland JA, O apos Brien J, Jayson MI. Nerve ingrowth into diseased intervertebral disc in chronic back pain. *Lancet*. Jul 19 1997;350(9072):178-181. doi:10.1016/s0140-6736(97)02135-1

24. Brisby H. Pathology and possible mechanisms of nervous system response to disc degeneration. *J Bone Joint Surg Am*. Apr 2006;88 Suppl 2:68-71. doi:10.2106/JBJS.E.01282

25. Lama P, Le Maitre CL, Harding IJ, Dolan P, Adams MA. Nerves and blood vessels in degenerated intervertebral discs are confined to physically disrupted tissue. *J Anat*. Jul 2018;233(1):86-97. doi:10.1111/joa.12817

26. Krock E, Rosenzweig DH, Chabot-Dore AJ, et al. Painful, degenerating intervertebral discs up-regulate neurite sprouting and CGRP through nociceptive factors. *J Cell Mol Med*. Jun 2014;18(6):1213-25. doi:10.1111/jcmm.12268

27. Freemont AJ, Peacock TE, Goupille P, Hoyland JA, O'Brien J, Jayson MI. Nerve ingrowth into diseased intervertebral disc in chronic back pain. *Lancet*. Jul 19 1997;350(9072):178-81. doi:10.1016/s0140-6736(97)02135-1

28. Risbud MV, Shapiro IM. Role of cytokines in intervertebral disc degeneration: pain and disc content. Review. *Nature reviews Rheumatology*. Jan 2014;10(1):44-56. doi:10.1038/nrrheum.2013.160

29. Burke JG, Watson RWG, McCormack D, Dowling FE, Walsh MG, Fitzpatrick JM. Intervertebral discs which cause low back pain secrete high levels of proinflammatory mediators. *The Journal of bone and joint surgery British volume*. 2002;84(2):196-201.

30. Freemont AJ. The cellular pathobiology of the degenerate intervertebral disc and discogenic back pain. *Rheumatology (Oxford)*. Jan 2009;48(1):5-10. doi:10.1093/rheumatology/ken396

31. Grunhagen T, Wilde G, Soukane DM, Shirazi-Adl SA, Urban JPG. Nutrient Supply and Intervertebral Disc Metabolism. *Bone and Joint Surgery*. 2006 2006;88-A:30-35. doi:10.2106/JBJS.E.01290

32. Clayton SW, Walk RE, Mpofu L, Easson GWD, Tang SY. Sex-specific divergences in the types and timing of infiltrating immune cells during the intervertebral disc acute injury response and their associations with degeneration. *Osteoarthritis Cartilage*. Feb 2025;33(2):247-260. doi:10.1016/j.joca.2024.10.002

920 33. Johnson ZI, Schoepflin ZR, Choi H, Shapiro IM, Risbud MV. Disc in flames: Roles of TNF-
921 alpha and IL-1beta in intervertebral disc degeneration. *Eur Cell Mater*. Sep 21 2015;30:104-16;
922 discussion 116-7. doi:10.22203/ecm.v030a08
923 34. Millecamps M, Tajerian M, Naso L, Sage EH, Stone LS. Lumbar intervertebral disc
924 degeneration associated with axial and radiating low back pain in ageing SPARC-null mice. *PAIN®*.
925 Jun 2012;153(6):1167-1179. doi:10.1016/j.pain.2012.01.027
926 35. Oehme D, Goldschlager T, Ghosh P, Rosenfeld JV, Jenkin G. Cell-Based Therapies Used to
927 Treat Lumbar Degenerative Disc Disease: A Systematic Review of Animal Studies and Human
928 Clinical Trials. *Stem Cells Int*. 2015;2015:946031. doi:10.1155/2015/946031
929 36. Barbe MF, Chen FL, Loomis RH, et al. Characterization of pain-related behaviors in a rat
930 model of acute-to-chronic low back pain: single vs. multi-level disc injury. *Front Pain Res*
931 *(Lausanne)*. 2024;5:1394017. doi:10.3389/fpain.2024.1394017
932 37. Ruzankina Y, Pinzon-Guzman C, Asare A, et al. Deletion of the developmentally essential
933 gene ATR in adult mice leads to age-related phenotypes and stem cell loss. *Cell Stem Cell*. Jun 7
934 2007;1(1):113-126. doi:10.1016/j.stem.2007.03.002
935 38. Gerber HP, Hillan KJ, Ryan AM, et al. VEGF is required for growth and survival in neonatal
936 mice. *Development*. Mar 1999;126(6):1149-59. doi:10.1242/dev.126.6.1149
937 39. Madisen L, Zwingman TA, Sunkin SM, et al. A robust and high-throughput Cre reporting and
938 characterization system for the whole mouse brain. *Nat Neurosci*. Jan 2010;13(1):133-40.
939 doi:10.1038/nn.2467
940 40. Liu JW, Lin KH, Weber C, et al. An In Vitro Organ Culture Model of the Murine
941 Intervertebral Disc. *Journal of visualized experiments : JoVE*. Apr 11 2017;(122):e55437-e55437.
942 doi:10.3791/55437
943 41. Walk RE, Moon HJ, Tang SY, Gupta MC. Contrast-enhanced microCT evaluation of
944 degeneration following partial and full width injuries to the mouse lumbar intervertebral disc. *Sci Rep*.
945 Sep 16 2022;12(1):15555. doi:10.1038/s41598-022-19487-9
946 42. Andersson GB. Epidemiological features of chronic low-back pain. *Lancet*. Aug 14
947 1999;354(9178):581-5. doi:10.1016/S0140-6736(99)01312-4
948 43. Atlas SJ, Deyo RA. Evaluating and managing acute low back pain in the primary care setting. *J*
949 *Gen Intern Med*. Feb 2001;16(2):120-31. doi:10.1111/j.1525-1497.2001.91141.x
950 44. Melgoza IP, Chenna SS, Tessier S, et al. Development of a standardized histopathology
951 scoring system using machine learning algorithms for intervertebral disc degeneration in the mouse
952 model-An ORS spine section initiative. *JOR Spine*. Jun 2021;4(2):e1164. doi:10.1002/jsp2.1164
953 45. Scheller E, Brazill JM, Lorenz M. Spatial mapping and contextualization of axon subtypes
954 innervating the long bones of C3H and B6 mice. protocolsio2021.
955 46. Hodgdon KE, Hingtgen CM, Nicol GD. Dorsal root ganglia isolated from Nf1+/- mice exhibit
956 increased levels of mRNA expression of voltage-dependent sodium channels. *Neuroscience*. Mar 29
957 2012;206:237-44. doi:10.1016/j.neuroscience.2011.12.045
958 47. Roza C, Laird JM, Souslova V, Wood JN, Cervero F. The tetrodotoxin-resistant Na+ channel
959 Nav1.8 is essential for the expression of spontaneous activity in damaged sensory axons of mice. *J*
960 *Physiol*. Aug 1 2003;550(Pt 3):921-6. doi:10.1113/jphysiol.2003.046110
961 48. Bird EV, Christmas CR, Loescher AR, et al. Correlation of Nav1.8 and Nav1.9 sodium channel
962 expression with neuropathic pain in human subjects with lingual nerve neuromas. *Mol Pain*. Oct 21
963 2013;9:52. doi:10.1186/1744-8069-9-52
964 49. Walk RE, Tang SY. In vivo contrast-enhanced microCT for the monitoring of mouse thoracic,
965 lumbar, and coccygeal intervertebral discs. *JOR Spine*. Jun 01 2019;2(2)doi:10.1002/jsp2.1058

50. Lin KH, Wu Q, Leib D, Tang SY. A Novel Technique for the Contrast-Enhanced microCT Imaging of Murine Intervertebral Discs. *Journal of the mechanical behavior of biomedical materials*. Jun 2016;doi:10.1016/j.jmbbm.2016.06.003
51. Easson GWD, Savadipour A, Anandarajah A, et al. Modulation of TRPV4 protects against degeneration induced by sustained loading and promotes matrix synthesis in the intervertebral disc. *FASEB J*. Feb 2023;37(2):e22714. doi:10.1096/fj.202201388R
52. Goh J, Ladiges W. Voluntary Wheel Running in Mice. *Curr Protoc Mouse Biol*. Dec 2 2015;5(4):283-290. doi:10.1002/9780470942390.mo140295
53. Chaplan SR, Bach FW, Pogrel JW, Chung JM, Yaksh TL. Quantitative assessment of tactile allodynia in the rat paw. *J Neurosci Methods*. Jul 1994;53(1):55-63. doi:10.1016/0165-0270(94)90144-9
54. Sheahan TD, Siuda ER, Bruchas MR, et al. Inflammation and nerve injury minimally affect mouse voluntary behaviors proposed as indicators of pain. *Neurobiol Pain*. Aug-Dec 2017;2:1-12. doi:10.1016/j.ynpai.2017.09.001
55. Duraku LS, Hossaini M, Hoendervangers S, et al. Spatiotemporal dynamics of re-innervation and hyperinnervation patterns by uninjured CGRP fibers in the rat foot sole epidermis after nerve injury. *Mol Pain*. Aug 30 2012;8:61. doi:10.1186/1744-8069-8-61
56. Allen KD, Griffin TM, Rodriguiz RM, et al. Decreased physical function and increased pain sensitivity in mice deficient for type IX collagen. *Arthritis Rheum*. Sep 2009;60(9):2684-93. doi:10.1002/art.24783
57. Kamisli S, Karakurt A, Uyumlu AB, et al. Evaluation of the effects of novel nafimidone derivatives on thermal hypoalgesia in mice with diabetic neuropathy. *Balkan Med J*. Mar 2013;30(1):94-8. doi:10.5152/balkanmedj.2012.067
58. Samineni VK, Yoon J, Crawford KE, et al. Fully implantable, battery-free wireless optoelectronic devices for spinal optogenetics. *Pain*. Nov 2017;158(11):2108-2116. doi:10.1097/j.pain.0000000000000968
59. Jain S, Golden JP, Wozniak D, Pehek E, Johnson EM, Jr., Milbrandt J. RET is dispensable for maintenance of midbrain dopaminergic neurons in adult mice. *J Neurosci*. Oct 25 2006;26(43):11230-8. doi:10.1523/JNEUROSCI.1876-06.2006
60. Deacon RM. Measuring the strength of mice. *J Vis Exp*. Jun 2 2013;(76)doi:10.3791/2610
61. Meyer OA, Tilson HA, Byrd WC, Riley MT. A method for the routine assessment of fore- and hindlimb grip strength of rats and mice. *Neurobehav Toxicol*. Fall 1979;1(3):233-6.
62. Moon HJ, Yurube T, Lozito TP, et al. Effects of secreted factors in culture medium of annulus fibrosus cells on microvascular endothelial cells: elucidating the possible pathomechanisms of matrix degradation and nerve in-growth in disc degeneration. *Osteoarthritis and Cartilage*. 02/2014 2014;22(2):344-354. doi:10.1016/j.joca.2013.12.008
63. RE MHaB. Detecting outliers when fitting data with nonlinear regression – a new method based on robust nonlinear regression and the false discovery rate. *BMC Bioinformatics*. 2006;7(123)

List of Abbreviations

AF – Annulus Fibrosus
Ai9 – Cre-reporter expressing tdTomato fluorescent protein (Rosa-CAG-LSL-tdTomato)
ANOVA – Analysis of Variance
CEμCT – Contrast-Enhanced Micro-Computed Tomography
CLBP – Chronic Low Back Pain
CM – Conditioned Media
CTCF – Corrected Total Cell Fluorescence
C57BL/6J – Common inbred mouse strain
DAPI – 4′,6-Diamidino-2-Phenylindole (DNA stain)
DEG – Differentially Expressed Gene
DHI – Disc Height Index
DRG – Dorsal Root Ganglion
EC – Endothelial Cell
EDTA – Ethylenediaminetetraacetic Acid (chelating agent)
ELISA – Enzyme-Linked Immunosorbent Assay
EMCN – Endomucin (endothelial cell marker)
EMEM, ATCC – Eagle's Minimum Essential Medium, from American Type Culture Collection
ERT2 – Modified Estrogen Receptor Ligand Binding Domain (used in tamoxifen-inducible Cre systems)
EVF – Electronic Von Frey
FBS – Fetal Bovine Serum
FITC – Fluorescein Isothiocyanate dye
FSU – Functional Spinal Unit
HBSS – Hanks' Balanced Salt Solution
HMEC-1 – Human Microvascular Endothelial Cell Line
IL1β – Interleukin 1 Beta
IVD – Intervertebral Disc
LBP – Low Back Pain
LoxP – Locus of X-over P1 (recombination sites for Cre-Lox systems)
LSD – Least Significant Difference (statistical post hoc test)
MCDB – Molecular, Cell, and Developmental Biology
Nav1.8 – Voltage-Gated Sodium Channel (gene SCN10A) expressed in nociceptive neurons
NFkB – Nuclear Factor Kappa B
NGF – Nerve Growth Factor
NI/DI – Nucleus Attenuation Intensity/Disc Attenuation Intensity
NP – Nucleus Pulposus
OCT – Optimal Cutting Temperature Compound
PAP – Hydrophobic barrier pen
PBS – Phosphate-Buffered Saline
PGP9.5 – Protein Gene Product 9.5 (neuronal marker)
P/S – Penicillin/Streptomycin
ROI – Region of Interest
SCRAM – Scrambled siRNA (negative control)
SH-SY5Y – Human Neuroblastoma Cell Line
siRNA – Small Interfering RNA
SNT – Simple Neurite Tracer (ImageJ plugin)
TNFα – Tumor Necrosis Factor Alpha
TNT – Tris-NaCl-Tween buffer
TrKA – Tropomyosin Receptor Kinase A (NGF receptor)
TRPA1 – Transient Receptor Potential Ankyrin 1
TRPV1 – Transient Receptor Potential Vanilloid 1
UBC – Ubiquitin
VEGF – Vascular Endothelial Growth Factor
WT – Wild Type

Acknowledgments:

We acknowledge the support of the Washington University Musculoskeletal Research Center Structure and Function Core (Michael Brodt); Histology Core (Crystal Idleburg and Samantha Coleman); and Animal Behavior and Function Core. We also acknowledge Kelsey Collins and Washington University Pain Center Judith Golden for their training in behavioral assessments of pain. We thank Jenny McKensie and Evan Buettmann for assistance in working with the VEGFA-null animals. We thank the Washington University Genomics Technology Access Core (GTAC), and the Eve-tech for the multiplex ELISA analysis.

Funding:

This work was conducted with funding support from National Institute of Health:

National Institutes of Health grant R21AR081517 (ST/MG)

National Institutes of Health grant R01AR074441 (ST)

National Institutes of Health grant R01AR077678 (LS/ST)

National Institutes of Health grant P30AR074992 (MS)

National Institutes of Health grant S10OD028573 (MS)

Author contributions:

Conceptualization: RSP, SYT

Methodology: RSP, REW, HJM, ALL, ANS, SWC, LJ, LAS, MCG, SYT

Data Interpretation: Methodology: RSP, REW, HJM, ALL, ANS, SWC, LJ, LAS, MCG, SYT

Investigation: RSP, HJM, ALL, LJ, LAS, MCG, SYT

Visualization: RSP, HJM, ALL, SWC

Funding acquisition: LAS, MCG, SYT

Project administration: RSP

Supervision: SYT

Writing – original draft: RSP, HJM, ALL

Writing – review & editing: RSP, SWC, SYT

Competing interests:

Provisional Patent: 020859/US

Title: VEGFA INHIBITORS AS A TREATMENT FOR CHRONIC MECHANICAL ALLODYNIA

Co-inventors: RSP, HJM, MCG, SYT

Data and materials availability: All data, code, and materials used in the analysis must be available in some form to any researcher for purposes of reproducing or extending the analysis. Include a note explaining any restrictions on materials, such as materials transfer agreements (MTAs). Note accession numbers to any data relating to the paper and deposited in a public database; include a brief description of the data set or model with the number. If all data are in the paper and supplementary materials, include the sentence